Propagation channel model between unmanned aerial vehicles for emergency communications

Sathya Narayana Venkatasubramanian

School of Electrical Engineering

Thesis submitted for examination for the degree of Master of Science in Technology.

Espoo 10.01.2013

Thesis supervisor:

Prof. Antti Räisänen

Thesis instructors:

Dr.Eng Kenichi Takizawa

Dr.Eng Katsuyuki Haneda

Aalto University
School of Electrical
Engineering

AALTO UNIVERSITY
SCHOOL OF ELECTRICAL ENGINEERING

ABSTRACT OF THE
MASTER'S THESIS

Author: Sathya Narayana Venkatasubramanian

Title: Propagation channel model between unmanned aerial vehicles for emergency communications

Date: 10.01.2013 Language: English Number of pages:64

Department of Radio Science and Engineering

Professorship: Radio Engineering Code: S-26

Supervisor: Prof. Antti Räisänen

Instructors: Dr.Eng Kenichi Takizawa, Dr.Eng Katsuyuki Haneda

The aim of the thesis is to create a radio propagation channel model for communication between unmanned aerial vehicles (UAVs) during emergency scenarios. The propagation channel model is designed at 2.4 GHz based on ray-tracing simulations performed over the Sendai City terrain, Japan and over the sea.

During the post-disaster scenario with the loss of communication infrastructure and loss of power, it is essential to provide a means of communication to the people in the affected area. One of the possible solutions is to provide for a relay link from a functioning base station to the affected area using unmanned aerial vehicles. The relay link is established for every 3 km such that each UAV is circling with a radius of about 100 m over a given area. To establish such relay links, characterization of the radio propagation channel is essential in designing the communication systems.

The path loss at the desired frequency, effect of various multipath components occurring based on the terrain, small scale fading, the effect of Doppler shift due to the movement of the UAVs and the delay dispersion are characterized. The excess delay and coherence bandwidth are compared to the guard interval and sub-carrier spacing of IEEE 802.11g/n and 802.16 WiMAX standards. The channel modelling is performed for different altitudes of UAV operation (150 m and 500 m) for both horizontal and vertical polarizations of transmitting and receiving fields. The guard interval of 802.16 WiMAX systems is sufficient to prevent inter-symbol interference for all UAV propagation scenarios. Frequency flat fading occurs for each Orthogonal Frequency Division Multiplexing (OFDM) sub-carrier and frequency selective fading occurs over the entire channel bandwidth. In case of 802.11g/n systems, the guard interval is not sufficient for all propagation scenarios and flat fading for OFDM sub-carriers occurs at UAV altitudes of 150 m for typical cases. The effect of Doppler shift is detrimental for 802.16 OFDM systems.

Keywords: UAV relay, unmanned aerial vehicles, aerial propagation, radio propagation channel for UAV relays, emergency communications

Preface

I would like to thank Prof. Pertti Vainikainen for introducing me to propagation research and providing the opportunity to work on this topic. I would also like to extend my thanks to Dr. Kenichi Takizawa for proposing the topic and providing his valuable insight during the instruction of the thesis.

I would also like to thank Prof. Antti Räisänen for supervising the thesis and Dr. Katsuyuki Haneda for instructing the same. Thank you for your support and patience.

To all those friends and family in Finland, I wouldn't have been able to complete this thesis if not for you!

Otaniemi, 10.01.2013

Sathya Narayana Venkatasubramanian

Contents

List of Figures

List of Tables

Symbols

A	Field strength of direct component
A_e	Effective aperture
B_d	Doppler spread
B_c	Coherence bandwidth
d	Distance
E	Electric field
f_c	Carrier frequency
f_d	Doppler frequency
f_m	Maximum Doppler shift
G_r	Gain of receiving antenna
G_t	Gain of transmitting antenna
$h(t)$	Channel impulse response
h_r	Height of receiver
h_t	Height of transmitter
I_0	Bessel function of the zeroth order and first kind
K	Ricean K-factor
k	Propagation constant
l_i	Length of i^{th} multipath component
N	Number of multipath components
n	Pathloss exponent
n_i	Refractive index of i^{th} medium
PL	Path loss
P_r	Received power
P_t	Transmitted power
Q	Marcum Q function
R	Reflection coefficient
r^2	Correlation coefficient
S	Power density
s^2	Variance in error
T	Transmission coefficient
T_c	Coherence time
T_s	Symbol duration
v	Velocity
$x(t)$	Input signal
$y(t)$	Output signal
β	Wave number
Δh	Deviation in surface height
δ_ϕ	Phase difference
Δ_l	Path difference
Δ_f	Frequency variation
ϵ_0	Permittivity of free space
ϵ_r	Relative permittivity
θ_b	Brewster's angle

θ_i	Angle of incidence
θ_r	Angle of reflection
λ	Wavelength
μ_r	Relative permeability
ρ_s	Roughness factor
σ	Standard deviation
σ_{eff}	Effective conductivity
σ_t	RMS delay spread
τ_i	Excess delay of i^{th} multipath component
$\overline{\tau}$	Mean excess delay
ϕ_i	Phase of i^{th} multipath component
ω	Angular frequency

Abbreviations

2G	Second Generation
4G	Fourth Generation
AWGN	Additive White Gaussian Noise
BER	Bit Error Rate
CAP	Civil Air Patrol
EIRP	Equivalent Isotropic Radiated Power
FFT	Fast Fourier Transform
GSM	Global System for Mobile communications
H-H	Horizontal Transmitter - Horizontal Receiver
HALE	High Altitude, Long Endurance
ICI	Inter-Carrier Interference
KKE	Kozo Keikaku Engineering
LoS	Line of Sight
LTE	Long Term Evolution
NICT	National Institute of Information and Communications Technology
OFDM	Orthogonal Frequency Division Multiplexing
PDF	Probability Density Function
PDP	Power Delay Profile
PEC	Perfect Electric Conductor
PL	Path Loss
RMS	Root mean squared
RSSI	Received Signal Strength Identifier
SIR	Signal to Interference Ratio
SUAV	Small Unmanned Aerial Vehicle
TE	Transverse Electric
TM	Transverse Magnetic
UAV	Unmanned Aerial Vehicle
UHF	Ultra High Frequency
UMTS	Universal Mobile Telecommunications system
VHF	Very High Frequency
VSAT	Very Small Aperture Terminal
VOIP	Voice Over Internet Protocol
V-V	Vertical Transmitter - Vertical Receiver
WiMAX	Worldwide Interoperability for Microwave Access
WRC	World Radio Conference

1 Introduction

1.1 Motivation

In the current scenario, disasters like earthquakes, hurricanes, etc. leave a devastating imprint on the affected area. In this era where communication has become an invaluable requirement amongst people, emergency communications during such disasters play a major role in the response and recovery of the affected region. Disasters leave a trail of damages including that of power and communication infrastructure which will take time to be restored. Individual terminals like mobile phones are more likely to survive after the disaster as compared to larger infrastructure. Providing the people with access to a network for communication in the immediate aftermath of a disaster will go in a long way in the recovery process. The prime advantage of such communications is that it will provide a means of communication to the first response team and also for the people in the affected area to communicate with the authorities for help, to be provided with information or to contact people outside the affected area. One of the solutions to provide emergency communications is to provide connectivity by means of aerial relay links as the base stations in the affected area are devoid of power supply or heavily congested. To design suitable communication systems for the relay links, the propagation channel between the relays needs to be characterized. Hence, the objective of the thesis is to create a channel model to characterize relay links between unmanned aerial vehicles.

1.2 Airborne emergency communication technologies

The easiest way to restore communication links during emergency scenarios is by using airborne devices due to their quick deployment as accessibility to the affected areas may not be feasible for ground based solutions. There are a wide variety of options which provide for airborne relay links to connect the people in the affected area. Some of the feasible technologies mentioned in [1] are as follows:

- Small unmanned aerial vehicles (SUAVs) which are small, hand-launched and battery powered. They are capable of flying upto 150 m above ground level. Since they are small, they can support a single service or a single frequency band of operation for cellular services. They can also be pre-deployed or deployed easily in case of emergencies and they can stay airborne for several hours.

- Weather balloons can also be used as repeaters and allow use of more than one frequency band as they can bridge different repeater technologies but they cannot remain airborne for a very long time and have to be relaunched frequently.

- High Altitude, Long Endurance (HALE) unmanned vehicles which operate at higher altitudes (greater than 9100 m). They can operate for longer durations and carry larger payloads. They also can support geographically directed communications resulting in decrease of potential harmful interference and also in increase in capacity.

- Deployable suitcase systems which comprise of suitcase transceivers placed on low flying aircrafts can be used as repeaters to provide for relay links.

Technologies like quick-mounted antennas, repeaters, transmitter on wheels and satellite technologies are also potential technologies which can be used for emergency communications.

1.3 Requirements and challenges for emergency communication systems

This section deals with the challenges and requirements necessary to establish a reliable communication system accessible to both the rescue workers as well as the public in the affected area in the post-disaster scenario. The contents of this section are primarily based on [1, 2].

Communication acts as a backbone for emergency response. It affects the reaction time, command and control, response, recovery and operational efficiency of the rescue workers who are the first responders in case of any type of disaster. The speed of recovery is of very high priority in case of any emergency situation. Hence, there is a need to improve the communication infrastructure to cater to the people in the affected area and to provide voice, broadband connectivity and high speed data transfer to the affected regions. Some possible solutions to provide emergency communications are amateur radio, Citizen's Band radio, satellites and mobile cell sites. In the post disaster scenario, power might not be available for around 6-8 days which in turn affects the restoration and repair work of the necessary infrastructure. This could occur in the location of base stations or the infrastructure at the base stations may be damaged which will take time to recover.

The primary concerns regarding the implementation of emergency communication systems is to identify the target beneficiaries and also type of technology services to be provided to the people. Some possible uses of airborne devices for emergency communications are to provide for disaster reconnaissance, to provide real time video from the air, monitoring, rescue missions trunking and communication systems. It is also important that the day to day communication devices are operational.

Currently, in the United States, air borne repeaters with broadband multi-frequency antennas mounted on civil air patrol (CAP) aircrafts are used to connect to handheld radios used by guards during recovery. It is also important to provide information to

people regarding availability and location of resources. Wide area VHF communications are used by fire fighters for communication purposes. The cell phone networks are usually saturated due to large amount of users trying to access the system at the same time. Test system operations have already been performed at VHF, UHF and the 700/800 MHz band [2].

There is also a need to implement the terrestrial based roll call technology in airborne devices to identify the available functioning resources at a particular location and accessibility issues faced by the terrestrial system are overcome. VHF and UHF technologies are already available for land communications and Very Small Aperture Terminals (VSATs) are also used to provide for communication links. The networks have a high possibility to get overloaded. Hence there is a need to provide for a survivable network especially for the first responders.

The emergency call services should be improved from only voice to text messages, etc. A disadvantage of such systems is that they have limited capability providing only emergency communication to the authorities. A solution to such emergency communications is to design hastily formed networks which comprise of technologies like satellite communications, Wi-Fi, WiMAX (Worldwide Interoperability for Microwave Access), broadband internet and Voice over Internet Protocol (VOIP) technologies. These systems provide for an airborne wireless delivery option.

It is also important to identify the hotspots where coverage is required and instead of a single communication system, an ecosystem comprising of various platforms is preferred to provide a wide variety of services. Interoperability between various systems must also be considered so that there is a seamless integration between various technologies. Factors to be decided in implementation of such airborne communication technologies is to identify the scale of coverage of various platforms, type of payloads, their power consumption and scalability. With airborne technologies, new applications can also be delivered to smartphones. An inherent feature of the systems should be priority access to the network and queueing so that the people in immediate need and the first responders and rescue workers are provided with connectivity immediately. Situational awareness is also to be provided along with broadcast capability. The technology must be such that any low cost handset available could be used to access the network. A possibility is that the deployed network is initially provided to the first responders and rescue workers and then made available for public usage.

In the USA, the VHF/UHF/800 MHz/900 MHz frequencies can be used during such a scenario. The frequencies can by shared or reused with close spacing. It is very critical to avoid interference and the height of the system plays a major role. It is also important to limit the use of interoperability channels.

Another practical issue is the altitude of such airborne devices. A higher altitude provides for a wider footprint but then causes cell breathing which results in inter-

ference between various active devices. As the altitude of the airborne devices is decreased from satellite altitudes, the coverage and power levels to be transmitted are reduced. Lower altitudes provide smaller footprint and greater frequency reuse. An altitude between 300 m to 1500 m would be optimal for such scenarios. As the altitude increases, the interference radius also increases. While the coverage area and interference increases, path loss to target regions is also affected. The altitude also shouldn't be too low to restrict coverage.

The systems should be rugged and the aim should be to design the best possible solution for maximum number of people. Some people in the neighbouring area may be affected by interference. The limits and thresholds of interference should be decided based on the requirement.

Hence, with these challenges in mind, an aerial relay system needs to be established to provide for emergency communications.

1.4 System design challenges

In order to design emergency communication systems, the onboard electronics, operating frequency, technologies, coverage, payload size, weight, etc. need to be finalized. This section deals with some system level challenges in designing such communication systems.

The packaging of the electronics is also important since it is to operate on an airborne device and hence affects the scale onboard, coverage and number of available communication platforms. The RF front end systems should have high capability to provide a direct link from the source to destination or use repeaters for such systems. Directional antennas can also be used to identify the spot size. The range, bandwidth etc. are to be decided based on the requirements.

One possible system could be to implement a self contained standalone cell network with dynamic spectrum reuse and broadcast capability. These are suitcase systems supporting 40-50 users and connecting to satellites. Mesh networks can be implemented between such devices.

The frequency availability and licensing issues are to be addressed so that the regulatory issues are sorted beforehand and the system requirements of spectrum and bandwidth are decided so that the system can be designed. It is also important to allocate frequencies for emergency communications as spectrum availability is limited and the licensing issues need to be preplanned with the coordination of the regulatory authorities.

From a commercial standpoint, it is important to provide services ranging from 2G to 4G LTE over the airborne systems to provide coverage for the people. For such a system, a reliable high capacity backhaul is required so that the services can be

provided without any interruptions. Broad area coverage also results in larger traffic and also the latencies are higher due to the relay links. It is also required to provide an SOS mode wherein any subscriber can connect to the network to contact the emergency services. The link budgets, power management and Doppler effect are to be considered and addressed. It is also necessary to reduce the harmful interference which depends on the propagation characteristics. Restoring ground assets should be a priority. Very high aerial platforms drain the handset power. Hence, the altitude of the transmitters shouldn't be too high. Licensing coordination is required with the licensees in the area. Enough separation between cell sites is also required. Priority access must be provided along with flexibility in platforms. The restoration of ground platform without interference from the airborne platform with seamless handoff is vital in resuming the terrestrial communications.

1.5 Objective of the project

In this project, relay links using unmanned aerial vehicles (UAVs) are considered providing cellular connectivity to the disaster stricken area from an operating base station. For developing a communication relay link using UAVs, the radio propagation channel must be characterized between two UAVs at the required frequencies of operation so that the communication systems can be developed to meet the requirements. Establishing a relay link using UAVs involves communication via two types of propagation channels, i.e. the air-ground channel which is used to characterize the channel between an existing base station and the UAV as well as between the UAV and mobile terminals and the air-air channel between two unmanned aerial vehicles. Already available research provides for channel models characterizing the air-ground channels for various scenarios. There are no validated propagation channel models characterizing the radio wave propagation between the UAV relays. The objective of the thesis is to develop a propagation channel model for the UAV-UAV relay links. The designed channel model is developed based on ray tracing analysis for various terrains including cities, sea and hilly terrain.

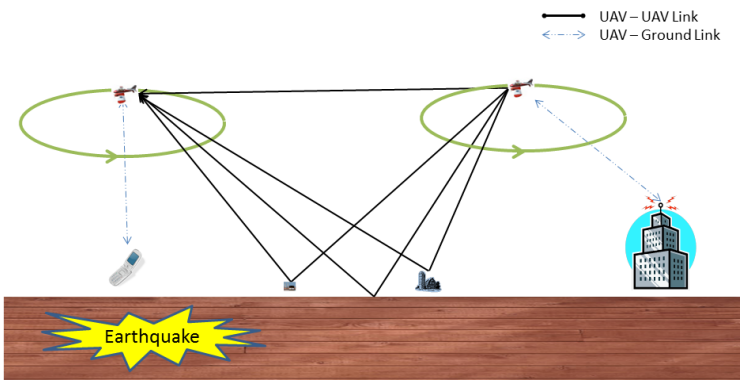

Fig. 1: Emergency communication link between two UAVs.

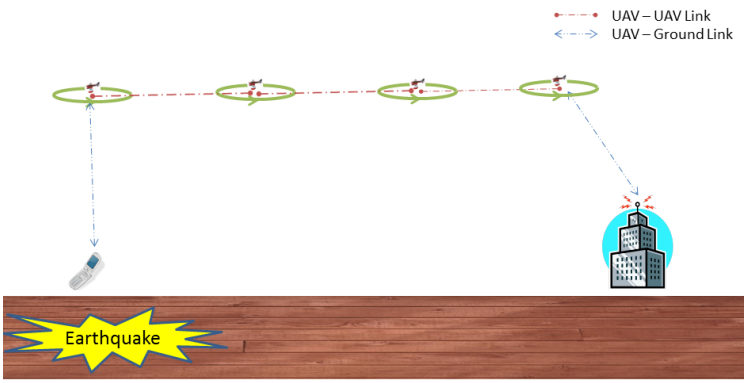

Fig. 2: Relay link using multiple UAVs.

The UAVs are to be operated such that they circle over a specific area with a radius of about 100 m. The performance of the UAV-UAV relay link is compared for different operational altitudes of 150 m and 500 m above the terrain level and for both horizontal and vertical polarizations of transmitting and receiving fields. A schematic representation of communication between two UAVs is shown in Fig. 1 and Fig. 2 depicts a relay link formed by UAVs. The number of relay UAVs depends upon the deployment scenario. The 2.4 GHz frequency band is proposed by National Institute of Information and Communications Technology (NICT), Japan for establishment of the relay links. The final frequency band decision is expected to be taken in the World Radio Conference (WRC) in 2015.

The outcome of the designed propagation channel model is to provide and analyze the following:

1. Path loss model at the desired operating frequencies,
2. Effect of fading due to multipath components,
3. Effect of Doppler shift due to the movement of the UAVs, and
4. Characteristics the propagation channel for different UAV heights and both polarizations.

The organization of the thesis is as follows. Chapter 2 discusses the propagation basics required for understanding the propagation channel and the basics of UAV channels is discussed in Chapter 3. Chapter 4 describes the simulations and Chapters 5 and 6 discuss the propagation channel model for UAV-UAV links and conclusion respectively.

2 Propagation basics

2.1 Introduction

Communication between a transmitter and receiver is largely dependent on the propagation channel characteristics between them. Hence, there is a need to create accurate generalized models to characterize the propagation channel. The propagation channel is usually characterized in a statistical manner based on measurements. This chapter is based on [3–6].

2.1.1 Propagation mechanisms

The phenomena encountered by a radio wave when it propagates from the transmitter to the receiver can be classified into the following namely:

- Free space propagation.
- Reflection from walls of buildings and smooth surfaces.
- Diffraction from building edges, rooftops and hills.
- Scattering from rough surfaces which are smaller than the wavelength (e.g. sea, rough ground, tree leaves and branches).

For a given link between a transmitter and receiver, the electromagnetic wave can travel in multiple paths due to the various propagation mechanisms listed above. These mechanisms are described in detail in Sections 2.2 to 2.6.

2.1.2 Elements of statistical channel model

Statistical models are required to characterize the propagation channel for system design. These models can be broadly classified into three categories based on the phenomenon which they characterize.

- Large scale path loss models are used to estimate the average signal strength for a given distance (electrically large) between the transmitter and the receiver.
- Shadowing model is used to estimate the attenuation of the signal due to electrically large obstacles.
- Small scale models are used to predict the fading characteristics, i.e. the fluctuation of the field strengths in the near vicinity of the receiver for very short distances (few wavelengths).

Sections 2.8 to 2.11 describe the elements used to characterize the channel model in detail.

2.2 Free space propagation

When an electromagnetic wave propagates through free space, i.e. the environment around the transmitter and the receiver is uncluttered, the wave is attenuated as the distance increases. The free space path loss between the transmitter and the receiver is given by the Friis formula as follows.

Consider a transmitter radiating a power P_t with an antenna gain of G_t. Hence, the $EIRP$ or the equivalent isotropic radiated power from the transmitter which is defined as the power an isotropic antenna would produce with the peak power density in the direction of maximum antenna gain and is given by

$$EIRP = P_t G_t \tag{1}$$

At a distance of d from the transmitter, the power density is given by the expression

$$S = \frac{EIRP}{4\pi d^2} \tag{2}$$

The gain of the receiver antenna is related to the effective aperture which represents the effective area of the receiver to receive the incoming signal. If G_r is the gain of the receiver antenna, the effective aperture given by A_e

$$A_e = \frac{\lambda^2 G_r}{4\pi} \tag{3}$$

where λ refers to the wavelength.

Hence, the received power at the receiver is

$$P_r = EIRP \times A_e = \frac{P_t G_t G_r \lambda^2}{(4\pi d)^2} \tag{4}$$

From the expression for the received power, the free space path loss can be computed as the ratio of the received power to that of the transmitted power and is usually expressed in decibels. If the gain of both the transmitter and receiver antennas are assumed to be 1, the path loss is expressed as

$$PL = \frac{\lambda^2}{(4\pi d)^2} \tag{5}$$

2.3 Reflection

Whenever an electromagnetic wave comes into contact with a smooth surface, i.e. the surface is very large as compared to the wavelength, a portion of the wave is transmitted and another portion is reflected back in the incident medium. This reflected component from a surface is called as the specular component and is one of the primary components of a multipath environment. The signal strength of the

reflected wave depends on two factors namely, the angle of incidence and the electric parameters of the surface, i.e. the complex relative permittivity of the dielectric material. The angle of incidence and reflection are based on laws of reflection. If the reflecting surface is a metal, i.e. a perfect electric conductor (PEC), the entire incident signal is reflected according to the laws of reflection whereas when the surface is a dielectric, it is lossy and the reflected signal is reduced in strength.

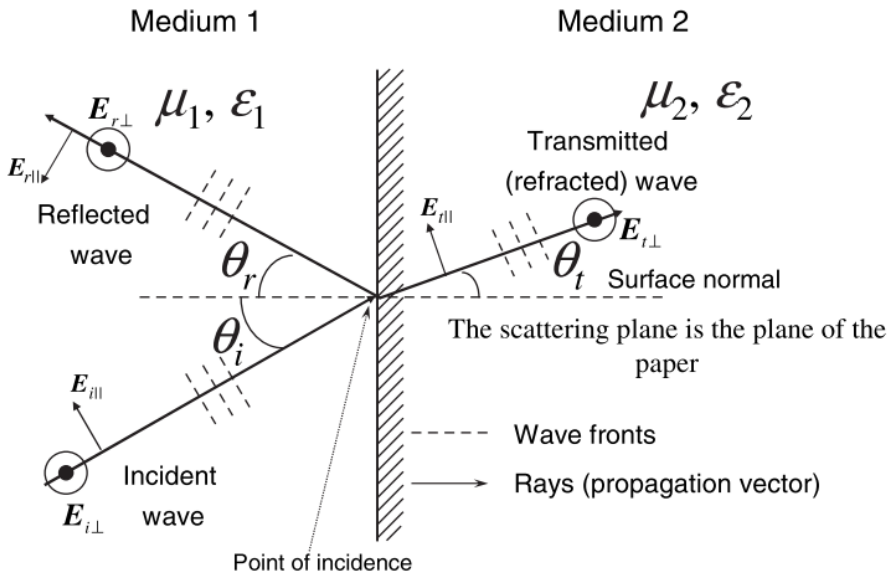

Fig. 3: Oblique plane wave incidence on a smooth boundary [3].

The strength of the reflected and transmitted waves are determined by the reflection and transmission coefficients which are dependent on the factors mentioned above. Fig. 3 shows the refection of a plane wave when it is incident on a smooth surface. The reflection coefficient is the ratio of the reflected electric field to the incident electric field. They are also dependent on the polarization of the incoming signal, i.e. the direction of the incident electric field and classified as transverse electric (TE) and transverse magnetic (TM) and are given by the expressions [3]

$$R_{TE} = \frac{\sin\theta_i - \sqrt{\epsilon - \cos^2\theta_i}}{\sin\theta_i + \sqrt{\epsilon - \cos^2\theta_i}} \qquad R_{TM} = \frac{\epsilon\sin\theta_i - \sqrt{\epsilon - \cos^2\theta_i}}{\epsilon\sin\theta_i + \sqrt{\epsilon - \cos^2\theta_i}} \tag{6}$$

$$T_{TE} = \frac{2\sqrt{\epsilon - \cos^2\theta_i}}{\sin\theta_i + \sqrt{\epsilon - \cos^2\theta_i}} \qquad T_{TM} = \frac{2\sqrt{\epsilon - \cos^2\theta_i}}{\epsilon\sin\theta_i + \sqrt{\epsilon - \cos^2\theta_i}} \tag{7}$$

In equations (6) and (7), the complex relative permittivity is defined by

$$\epsilon = \epsilon_r^{'} - j\epsilon_r^{''} = \epsilon_r^{'} - j\frac{\sigma_{eff}}{\omega\epsilon_0} \tag{8}$$

where ω refers to the angular frequency of the propagating wave and σ_{eff} refers to the effective conductivity of the dielectric.

It can be observed that, when the angle of incidence increases from 0° to 90°, the magnitude reflection coefficient for the vertical polarization decreases and reaches a minimum value for a particular angle of incidence called Brewster's angle after which again it increases. This also results in a phase change in the reflected signal. Brewster's angle depends on the refractive indices of the medium and hence the relative permittivity and is defined by the formula

$$\theta_b = \tan^{-1} \frac{n_2}{n_1} \tag{9}$$

where n_1 and n_2 refer to the refractive indices of the mediums. In case of reflection from obstacles like buildings and ground, n_1 is 1 due to free space and n_2 refers to the refractive index of the object and hence its relative permittivity. The refractive index is equal to the square root of the relative permittivity as the relative permeability μ_r is considered as 1.

Table 1 provides the standard electrical parameters of ground and water at 2 GHz [7].

Table 1: Typical Electrical Parameters at 2 GHz [7]

Surface	Effective conductivity (S/m)	Relative permittivity
Very dry ground	0.00075	3
Medium dry ground	0.125	15
Wet ground	0.4	25-30
Sea water	6	70
Fresh water	0.6	80

2.4 Two ray model

The free space path loss model is valid only when there is an unobstructed line of sight (LoS) path between the transmitter and the receiver and no objects in the first Fresnel zone. In a typical environment, unless highly directive and narrow beam antennas are used at both the transmitter and receiver, multiple paths exist between the transmitter and receiver. Hence, a generalized two ray model is used to characterize the channel where the received signal consists of a LoS component and a component resulting from the ground reflections. Although the power in the electromagnetic wave is spread over the Fresnel zone, it is difficult to model them in case of large propagation scenarios due to their computational complexity. Hence, ray theory is used to model the radio waves as rays to describe the propagation.

Let a transmitter and receiver be placed at heights h_t and h_r respectively separated by a horizontal distance d as shown in Fig. 4. The LoS path between the transmitter and receiver has a distance of d_{dir} and is the first component arriving at the receiver.

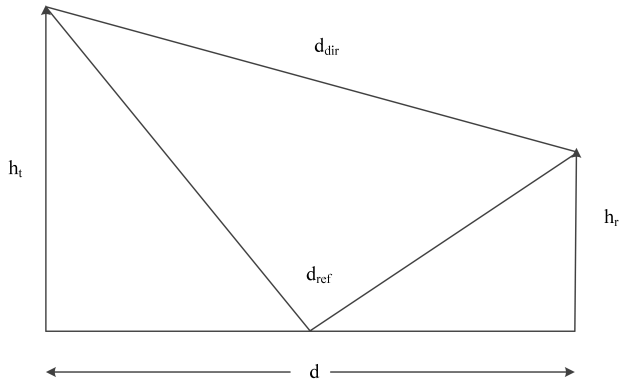

Fig. 4: Two ray model.

The reflected component travels towards the ground from the transmitter and gets reflected at a point on the ground based on the laws of reflection and then reaches the receiver. The total distance covered by the reflected ray is represented by d_{ref}. Since the path covered by the reflected ray is longer than that of the direct ray, there is an excess delay at the receiver after the arrival of the direct component. In practice, there may be more than one reflected ray arriving at the receiver depending upon the terrain profile.

Consider E_0 as the voltage at the input of the transmitter antenna port and let $f_1(\theta_1)$ and $f_2(\theta_2)$ represent the radiation pattern of the transmitter and receiver antennas respectively where θ_1 and θ_2 refer to the direction of the transmitted and received paths at the corresponding antennas. The electric field at the receiver due to the direct component for both TE and TM polarizations can be expressed as

$$E_{direct} = E_0 \frac{\lambda}{4\pi d_{dir}} e^{-jkd_{dir}} f_1(\theta_1) f_2(\theta_2) \tag{10}$$

The transmitter radiates in all directions depending upon the radiation pattern of the transmitter antenna, $f_1(\theta_1)$. Apart from the direct ray that reaches the receiver directly, the signal is also transmitted towards the ground which are then reflected back from the surface of the earth based on the laws of reflection. To characterize the reflection from the ground, the incident ray is considered to be a plane wave locally and the reflection coefficient is computed as mentioned in Section 2.3 to calculate the field strength of the corresponding reflected path at the receiver. Hence, the received signal of a ground reflected component is given by

$$E_{ref} = RE_0 \frac{\lambda}{4\pi d_{ref}} e^{-jkd_{ref}} f_1(\theta_1) f_2(\theta_2) \tag{11}$$

where R refers to the reflection coefficient and is calculated based on the angle of incidence and the electrical parameters of the ground at the corresponding location. It depends on the polarization of the incident wave. If isotropic antennas are used, then the channel can be characterized independent of the antenna effects, i.e. $f_1(\theta_1)$ and $f_2(\theta_2)$ are equal to 1.

Thus, the total field at the receiver is given by the vector sum of the individual fields produced by different components as

$$E_{tot} = E_{direct} + E_{ref} = E_0 \left(\frac{\lambda}{4\pi}\right) \left(\frac{e^{-jkd_{dir}}}{d_{dir}} + R\frac{e^{-jkd_{ref}}}{d_{ref}}\right) \tag{12}$$

From equation (12), it can be seen that the overall received power ($|E_{tot}|^2$) depends upon the phase in which the different components combine. If the transmitted power is known, the received power can then be calculated for the given link.

2.5 Diffraction

The concept of diffraction has its basis in the Huygens principle. According to the Huygens principle, every point on a wavefront produces spherical wavelets which results in a new secondary wavefront along the direction of propagation. Diffraction occurs when an incident wave encounters a sharp edge like building rooftops, edges in urban environments and hills in rural environments. Due to the presence of the secondary wavelets, even though LoS path is not available due to the presence of an obstacle, the wave propagates to the region behind the obstacle as shown in Fig. 5. This phenomenon is usually described as bending of the propagating wave around an obstacle.

The extent of diffraction depends upon the incident signal and the characteristics of the obstacle and the extent to which it obstructs the Fresnel zone. The uniform geometric theory of diffraction is used to characterize the diffraction and compute the field strengths in shadowed locations using diffraction coefficients which are also dependant on the polarization of the wave. In case of propagation over hilly terrain, when an incident ray bends over a hill top, the received signal strength will be minimal at the valley on the other side of the hill and increase as the height increases. This effect is similar in case of propagation in urban environment with large buildings.

2.6 Scattering

Scattering is a phenomenon occurring when the propagating wave encounters a rough surface. As level of roughness increases, the amount of scattering increases and the energy from the specular reflected component is reduced. It occurs when the size of the object or obstacle is comparable to that of the wavelength of the incident wave. The amount of scattering increases for angle of incidence varying from the grazing angle to perpendicular incidence.

Consider two adjacent propagating waves impinging a smooth surface. As the surface of the obstacle is smooth, the phase shift between the two adjacent waves is similar whereas in case of rough surfaces, the distance travelled by one wave might be larger as compared to the other due to the roughness of the surface. Hence as the level of roughness is higher, the phase shift also increases. Generally phase shifts of

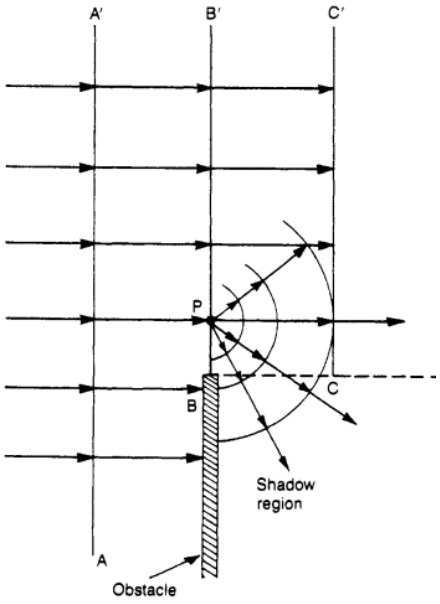

Fig. 5: Bending of incident wave due to diffraction : Huygens principle [6].

upto 90° are considered as smooth whereas to model the propagation phenomenon more accurately, a criterion called the Rayleigh criterion is used to characterize whether a given surface is rough or not. The Rayleigh criterion is defined by the formula

$$\Delta h = \frac{\lambda}{8 \cos \theta_i} \tag{13}$$

where Δh refers to the deviation in height in the surface, λ the wavelength and θ_i refers to the angle of incidence. The Rayleigh criterion defines the surface as rough if the deviation in phase shift is greater than $\lambda/8$. Fig. 6 shows the impact of surface roughness on scattering.

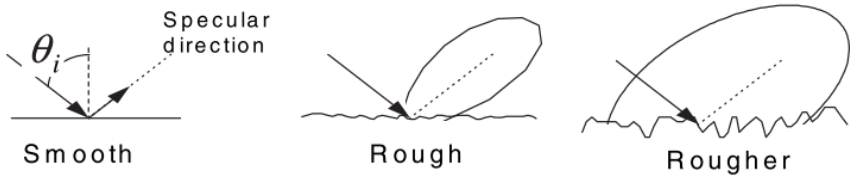

Fig. 6: Scattering due to surface roughness [3].

The effect of scattering on the specular reflected component can be characterized by a roughness factor which when multiplied with the reflection coefficient of the specular component, provides for the reduced signal strength of the reflected ray. The roughness factor can be characterized as a gaussian distributed random variable

for a given height with local mean and a standard deviation given by σ_s as

$$\rho_s = \exp\left[-8\left(\frac{\pi\sigma_s \sin\theta_i}{\lambda}\right)^2\right] \tag{14}$$

Based on measured results, the formula for surface roughness was modified as

$$\rho_s = \exp\left[-8\left(\frac{\pi\sigma_s \sin\theta_i}{\lambda}\right)^2\right] I_0\left[-8\left(\frac{\pi\sigma_s \sin\theta_i}{\lambda}\right)^2\right] \tag{15}$$

where I_0 refers to the Bessel function of the zeroth order and first kind [4].

Hence, the reflection coefficient of the specular component can be given by

$$R_{rough} = \rho_s R \tag{16}$$

In case of urban propagation, structures like walls and roofs of buildings are not smooth and contain irregularities like windows, etc. These irregularities also cause scattering of the incident radiation instead of a single specular component and contributes to the total field at a receiver location. If objects like vehicles are present on the road, they also contribute to scattering of the incident signal.

2.7 Depolarization

The polarization of a propagating radio wave is defined by the direction of the electric field vector. Every antenna radiates the electromagnetic wave with a particular polarization. In case of co-polarization, the polarization of the receiver antenna is the same as that of the transmit antenna. In case of cross-polarization, the polarization of the receiver antenna is orthogonal to that of the transmit antenna. Due to the effect of scattering and diffraction, along with attenuation of the signal, the polarization of the signal might undergo changes and hence at the receiver, both the co-polarized and the cross-polarized components may be present even though the signal was transmitted in a particular polarization. This is known as depolarization of the signal. This can also occur due to small objects like cars, posts, etc. The signal level of the cross polarized component is usually lower than that of the co-polarized component but in some cases of mobile reception, both the components may be of near equal strength [5].

2.8 Large scale path loss model

As we have seen in the earlier sections on how the various environmental phenomena affect the propagation of radio waves, it is important to have parameters to characterize their impact on system design. The large scale path loss model is one such parameter used to characterize the path loss as a function of the log-distance between the transmitter and the receiver. The path loss is expressed in decibel scale as

$$PL(dB) = PL_0(dB) + n10\log d \tag{17}$$

where d is the Tx-Rx distance in metres, PL is the path loss for distance d, n refers to the path loss exponent which depends upon the environment clutter and PL_0 refers to the path loss at a close-in distance (e.g. 1 m) which provides the y-intercept of the plot. The reference distance can also be in kilometres in which case the distance d is also in km. In practical scenarios, when path loss modelling is done, the small area average is plotted and a least mean squared (LMS) error fit is used to create the path loss model and the corresponding parameters. When the order of distances are small, the path loss at 1 m distance is computed from the free space model and used as the y-intercept for the model. When the order of distances is large, the measurement data could be used for the LMS fit for the data. The antenna effects like directivity are decoupled from the measured data to create the path loss model.

2.9 Shadowing

The path loss for a given distance varies for different locations. This is primarily due to the change in the surrounding environment between the different locations or presence of obstacles which attenuates the signal passing through them. This deviation in the path loss is known as shadowing. It affects the signal strength of the various multipath components and hence, creates variations in the path loss. This additional path loss is characterized by a Gaussian distributed random variable $X(dB)$ with a standard deviation of σ and represents the effect of shadowing. This is known as log-normal shadowing. Hence, the path loss formula is modified as

$$PL(dB) = PL_0(dB) + n10\log d + X(dB) \tag{18}$$

2.10 Impulse response

The impulse response is a metric used to characterize the performance of a channel for a given input signal. It is primarily used for the wideband characterization of systems. The impulse response is the dual of the frequency response of the channel and hence in field measurements, the frequency response is obtained and the impulse response is then obtained using inverse Fourier transform. This is due to the fact that the channel is modelled as a linear filter with a time varying impulse response. The time variation is primarily due to the motion of the receiver or change in the environment hence altering the channel characteristics.

The output signal $y(t)$ for a given input signal $x(t)$ at a given time instant t can be obtained by convolving the input signal with the impulse response of the channel $h(d,t)$ where d refers to the distance due to the motion of the receiver.

$$y(t) = x(t) * h(d,t) = \int_{-\infty}^{\infty} x(\tau)h(d,t-\tau) \tag{19}$$

To simplify the characterization of the channel impulse response, the channel is assumed as time invariant and can be expressed as the sum of the different multipath

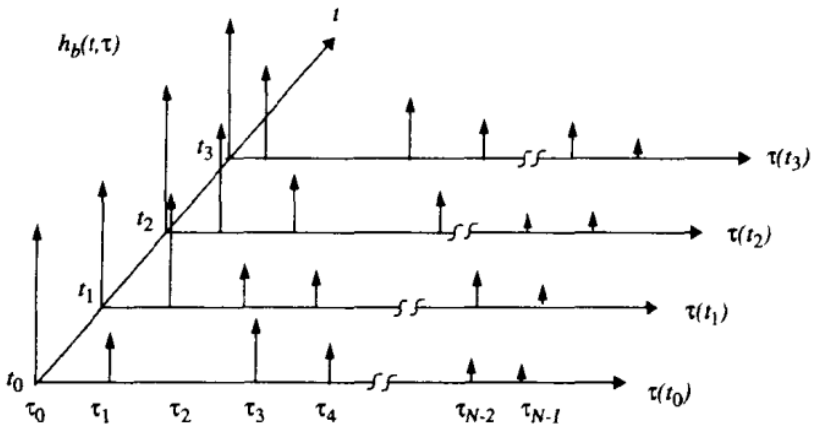

Fig. 7: Impulse response of a channel [4].

components with varying amplitude, phase and arrival time and expressed as

$$h(t) = \sum_{i=1}^{N} a_i e^{j\phi_i} \delta(t - \tau_i), \tag{20}$$

where $h(t)$ refers to the impulse response at a given time instant, the number of multipath components varying from 1 to N, $a_i e^{j\phi_i}$ refers to the complex amplitude and phase of the multipath component and τ_i refers to the delay of the i^{th} multipath component with respect to the first arriving component.

The power delay profile (PDP) is defined as the absolute square of the impulse response and shows the relative strength of each multipath component compared to the first arriving component.

2.11 Small scale fading

As we have seen in Sections 2.3 - 2.6, the effect of reflection, diffraction and scattering result in reception of multipath components at the receiver. The free space model and other shadowing and path loss models [3–6] are used to characterize the large scale path loss. Another major phenomenon which has to be characterized is the small scale fading. The impact of small scale fading can be broadly classified as [4]

- Multipath fading which refers to the fluctuation in the received signal due to the combining of various multipath components which arrive with different phases.
- Doppler dispersion which refers to the deviation or spread in the frequency of the received signal due to the relative motion of the transmitter and receiver as well as the motion of the objects in the surrounding.
- Delay dispersion which refers to the delayed arrival of the various multipath components at the receiver resulting in spreading of the received signal.

2.11.1 Multipath fading

At the receiver, the received signal comprises of different components arriving from different directions. The total received signal strength at a given location is computed by the sum of the individual field strengths of the various multipath components arriving at the receiver. Hence, the total field is expressed as

$$E_{tot} = \sum_i E_i e^{j\beta l_i} \tag{21}$$

where β is the wave number given by $\frac{2\pi}{\lambda}$ and l_i refers to the length of each path of taken by the signal to arrive at the receiver and E_i refers to the field strength at the receiver for the corresponding arrival path. The direct ray which has the shortest path length is the least attenuated whereas the signal strength of all the other paths occurring due to reflection, diffraction or scattering are attenuated due to the corresponding phenomenon. The total path length of each of the multipath components is greater than that of the direct component and hence, their corresponding field strength is also lower due to the interactions of the wave with obstacles in the propagating path along with the excess distance travelled. It can be observed that when all these components combine in phase, due to the various path lengths, the overall field strength can be increased or decreased depending on whether the phases combine in a constructive or destructive manner. If the receiver is moved by a short distance, the length of the arrival paths change and also the phase especially when the frequency of the propagating wave is high as the wavelength is very small as compared to the propagation distance. This results in a change in the overall field strength as compared to the previous location and this phenomenon is called small scale fading.

To characterize the effect of small scale fading, various types of fading distributions are used depending upon the scenario. Some common fading distributions are given below.

Rayleigh distribution The Rayleigh distribution is used to characterize small scale fading of a signal when there is no LoS component at the receiver or to characterize the fading of a particular multipath component. The probability density function (PDF) and cumulative distribution function (CDF) of the Rayleigh distribution are given by

$$PDF : p(r) = \begin{cases} \frac{r}{\sigma^2} \exp\left(-\frac{r^2}{2\sigma^2}\right) & \text{for } (0 \leq r \leq \infty) \\ 0 & \text{for } (r < 0) \end{cases}, \tag{22}$$

$$CDF : P(r) = 1 - \exp\left(-\frac{r^2}{2\sigma^2}\right). \tag{23}$$

where r is a random variable representing the amplitude of a complex number whose real and imaginary parts are random variables with normal distribution.

Rician distribution The Rician distribution is another probability distribution which is primarily used to characterize small scale fading in the presence of a LoS component with a significantly higher strength as compared to the other multipath components. The Rician fading depends upon the parameter K or the Rician K-factor which is defined as the ratio of the power of the LoS component to that of the variance of the multipath components and is given by the expression

$$K(dB) = 10\log_{10}\left(\frac{A}{2\sigma^2}\right), \tag{24}$$

where A is the field strength of the LoS component and σ^2 refers to the variance.

The PDF and CDF are given by the expressions

$$PDF : p(r) = \begin{cases} \frac{r}{\sigma^2}\exp\left(-\frac{(r^2+A^2)}{2\sigma^2}\right) I_0\left(\frac{Ar}{\sigma^2}\right) & \text{for } (0 \le r \le \infty) \\ 0 & \text{for } (r < 0) \end{cases}, \tag{25}$$

where I_0 is a zeroth order Bessel function of the first kind.

$$CDF : P(r) = 1 - Q\left(\frac{A}{\sigma}, \frac{r}{\sigma}\right), \tag{26}$$

where Q refers to the Marcum Q function.

2.11.2 Doppler dispersion

The Doppler effect refers to the shift in the frequency of the transmitted signal at the receiver due to its relative motion with respect to the transmitter. The impact of Doppler shift differs for each multipath component and depends on the direction of movement.

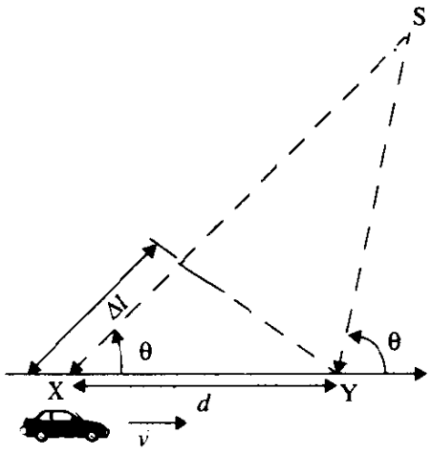

Fig. 8: Doppler effect [4].

Consider a receiver moving with a velocity v in a given direction with respect to a transmitter located at a distance from it as shown in Fig. 8. At a given time instant, the receiver is at a location X and receiving the transmitted signal with phase ϕ_i. If the receiver is stationary, there is no phase change as the path length remains constant. If the receiver moves to a point Y in time δt such that the distance between the points X and Y is d, there is a variation in the path length between the Tx and Rx. If the receiver moves away from the transmitter, there is a delay in the received phase at point Y as compared to the signal at point X. Due to this, the rate of phase change is reduced and hence, there is a decrease in the frequency. If the receiver moves towards the transmitter, the opposite effect takes place resulting in an increased phase change and thus an increase in frequency. This effect can be explained mathematically as follows.

If the path difference for the two paths between the transmitter and receiver is given by Δl, it can be expressed as $\Delta l = d\cos\theta$ where θ refers to the angle between the path and the ground in the direction of receiver movement as shown in Fig 8. Hence, the phase difference at the receiver is given by

$$\delta\phi = \frac{2\pi\Delta l}{\lambda} = \frac{2\pi v\delta t}{\lambda}\cos\theta \tag{27}$$

where v is the velocity of the receiver.

Hence, the variation in frequency is given by differentiating the phase w.r. to time as

$$\delta f = \frac{1}{2\pi}\frac{\delta\phi}{\delta t} = \frac{v}{\lambda}\cos\theta \tag{28}$$

This variation in frequency is called the Doppler frequency and as it an be seen, depending upon the direction of movement, δf is positive or negative, thereby increasing or decreasing the frequency. Two parameters called Doppler spread and coherence time are used to characterize the Doppler effect. When a receiver is moving with a relative velocity with respect to the transmitter, the Doppler shift f_d is calculated based on the above formula. The spectrum of the received signal around a carrier f_c has components varying from $f_c - f_d$ to $f_c + f_d$. This corresponds to a bandwidth, $B_d = 2f_d$ and is known as the Doppler spread. If the relative velocity changes, the Doppler shift and hence, the Doppler spread varies.

To characterize the time variation of the frequency dispersiveness of the channel, a parameter called coherence time is introduced. This depends upon the maximum Doppler shift which is in turn dependant upon the relative velocity of the receiver. The coherence time is proportional to the inverse of the maximum Doppler shift and as a rule of thumb, is given by the formula [4]

$$T_c = \sqrt{\frac{9}{16\pi {f_m}^2}} \tag{29}$$

Based on the Doppler shift, the small scale fading is characterized as slow fading and fast fading. Fast fading occurs when the coherence time is smaller than the symbol duration and the channel impulse response will have rapid variations within the symbol duration. In case of slow fading, the effect of the Doppler shift is negligible as the variation of the channel impulse response is slow compared to the symbol duration i.e. the symbol duration is smaller than the coherence time.

2.11.3 Delay dispersion

When multipath propagation occurs in the environment, due to the different path lengths travelled by the various components, the arrival time at the receiver is different for each path. Due to this, there is a time dispersion as various components of the same signal arrive at the receiver with different signal strengths and time delays. If some multipath components are delayed more than the time window at the receiver, then intersymbol interference occurs as the delayed component of the previous signal affects the next received symbol. Hence, delay dispersion modelling plays an important role in channel characterization as it also affects the system design.

The delay dispersion is characterized by three parameters namely, excess delay, the mean excess delay and root mean squared (RMS) delay spread. The excess delay is a parameter which is defined to compute the maximum delay of a multipath component with respect to the first arriving component such that they are above a certain power threshold with respect to the component with maximum signal strength. The excess delay can be calculated for various power threshold levels thereby providing for a detailed analysis of the channel characteristics.

The mean excess delay is defined by the formula

$$\overline{\tau} = \frac{\sum_k P(\tau_k)\tau_k}{\sum_k P(\tau_k)} \tag{30}$$

From the above expression, it can be observed that the mean excess delay is the first order moment of the power delay profile which denotes the power levels of the various multipath components with respect to the delay.

The RMS delay spread is defined as the square root of the second central moment and given by the expression,

$$\sigma_\tau = \sqrt{\overline{\tau^2} - (\overline{\tau})^2}, \tag{31}$$

where

$$\overline{\tau^2} = \frac{\sum_k P(\tau_k)(\tau_k)^2}{\sum_k P(\tau_k)}. \tag{32}$$

In the above equations, τ_k refers to the excess time delay of the k_{th} component with respect to the first component at the receiver (τ_0). $P(\tau_k)$ refers to the relative power

level of the received signal which is normalized to the peak value [4].

In case of a signal with various frequency components, the fluctuation in amplitude of each frequency component is different. This is known as frequency fading. A parameter called coherence bandwidth is used to characterize the frequency fading.

The coherence bandwidth of the channel is inversely proportional to the RMS delay spread. It refers to the maximum separation between two frequency components at the receiver which are correlated in amplitude. i.e. the signals within the coherent bandwidth are affected in the same manner in the channel. The attenuation of the signal by the channel remains constant while the phase varies linearly. Hence, a signal whose bandwidth is larger than the coherence bandwidth of the channel undergoes different levels of fading at different frequencies whereas a narrow band signal whose bandwidth is less than the coherence bandwidth undergoes similar type of fading. The coherence bandwidth can be determined approximately from the RMS delay spread for different correlation levels as $B_c = \frac{1}{50\sigma_\tau}$ for an amplitude correlation of 0.9 and $B_c = \frac{1}{5\sigma_\tau}$ for an amplitude correlation of 0.5 [4].

Hence, based on the coherence bandwidth, small scale fading can be characterized as flat fading and frequency selective fading. Flat fading occurs when the signal bandwidth is smaller than the coherence bandwidth and hence the delay spread is less than the symbol period. Such channels which undergo flat fading are referred to as narrowband channels. Frequency selective fading occurs when the signal bandwidth is greater than the coherence bandwidth and the delay spread is greater than the symbol duration. When the signal bandwidth significantly exceeds the coherence bandwidth, the channel is called as a wideband channel.

In case of flat fading, the entire signal may undergo deep fades and hence sufficient fade margin is required to overcome the deep fade. The entire signal is affected in the same manner and attenuated while retaining the shape of the envelope in the frequency domain. In frequency selective fading, since each frequency component is affected differently, it results in change in the spectrum of the received signal and the signal is distorted resulting in intersymbol interference.

3 UAV communication channels

3.1 Unmanned aerial vehicles

An unmanned aerial vehicle (UAV) is a device which functions either autonomously or by the remote control of a navigator. It is defined as a "powered, aerial vehicle that does not carry a human operator, uses aerodynamic forces to provide vehicle lift, can fly autonomously or be piloted remotely, can be expendable or recoverable and can carry a lethal or non lethal payload" [8].

3.2 Operation of UAV relay links

The aerial links can be broadly classified into two aspects namely, air-ground communications and air-air communications. UAV applications in general like reconnaissance, aerial surveying, remote sensing, exploration etc. require communication of data from the UAV to the ground. Along with the transmission of payload data, command and control operations also need to be performed between the ground control and the UAV. All these operations require reliable air-ground communications and there are already available models for propagation in the air-ground scenario. These models are available for a wide range of frequencies and can hence be used to model the links between the air and ground.

The use of UAVs and other aerial devices for relay links are an emerging technology and hence require the channel to be characterized for establishing communication links. As detailed in the following section, proposed models for characterizing air-air links are available based on theoretical models but the models are not validated with either numerical simulations or measurements. The thesis involves characterizing and validating the theoretical model with using ray tracing.

The following section provide an insight into the propagation channel characteristics and models available for both air-ground and air-air communication links.

3.3 Literature survey

The air-ground communication links provide for two types of links namely, one for transmission of payload information to the ground center which may be of high capacity based on the requirement and another for command and control. The command and control link could be established directly during take off and landing scenarios and then via satellite when the UAV is in operation depending upon its operational scenario [9].

In [9], both the air-ground and air-air links are considered and channel models are proposed for various operational scenarios like parking and taxi environments, take-off and landing and en-route scenarios. The paper also suggests typical and worst case parameters for the links based on measured data. From the proposed model,

flat and frequency selective fading channel emulators are derived and implemented in software and hardware. It deals with small area characterization dealing with propagation upto a few wavelengths. The propagation channel for the air-air links in the en-route scenario is characterized as a multipath channel with a LoS component and reflected delayed paths. The propagation channel is characterized as a two ray model and the fading is characterized using the Ricean distribution. For simplicity, the direct path modelled as a constant process and the reflected component is modelled as a Rayleigh process based on [10]. The typical Ricean K-factor which is a measure of the strength of the LoS component over that of the multipath components is computed as 15 dB for the air-air links. The Doppler effect is considered for a maximum velocity of 620 m/s for the air-air links and a non isotropic probability density function (Jake's distribution) is provided for the Doppler spread. Delays upto 1 ms and more are also possible for air-air links. The main frequency range for the discussion is at the VHF frequencies (118 to 137 MHz) and channel simulations are also performed for Orthogonal Frequency Division Multiplexing (OFDM) at 5 GHz with a bandwidth of 492 kHz. For the thesis, a large area characterization is required at 2.3 GHz. The characterization of the proposed multipath two ray model and the Doppler spread can be considered as an initial model for the propagation channel design.

The bit error rate (BER) performance of an 802.11a OFDM system at 5 GHz is analyzed in [11]. The OFDM communication is suggested for UAV swarms for communication between UAVs. The UAVs are considered to travel at a maximum relative velocity of 222 m/s and BER simulations are performed over an additive white gaussian noise (AWGN) channel as well as a frequency selective Rayleigh fading channel. The channel is frequency selective over the entire bandwidth but flat fading occurs over each sub-carrier. The simulation results show that for OFDM, there is a negligible effect in the performance of an AWGN channel and a 2 dB loss with a bit rate of 3×10^{-5} when the channel undergoes frequency selective fading. The air - air channel is characterized to have a large Doppler shift due to high speed of the UAVs, short coherence time and large inter carrier interference (ICI). There is also a loss of sub-carrier orthogonality and degradation of the ICI.

In [12], statistical models are provided for air-ground communications in urban environments. Terrain, building and foliage data for a 1.4 km $\times$ 1.4 km area in central Bristol was considered in developing the model. A mean building height of 11.7 m covering 28% of the total area and hilly terrain of standard deviation 17.5 m are considered. Crossed dipoles with circular polarization are used at the transmitter. For ray tracing simulations, the mobiles are located 1.5 m above ground level along with 9 aerial transmitters at 100 m height and path loss and shadowing angle are evaluated as a function of the elevation angle using a 3D outdoor ray tracing model. Various scenarios like LoS, Obstructed LoS (OLoS) and non-LoS cases are considered and mean path loss and shadowing models are derived. Simulations are performed at five frequencies between 200 MHz and 5 GHz (200 MHz, 1, 2, 2.5 and 5 GHz) to obtain spatial and temporal multipath data, Rician K-factor, RMS delay

spread and coherence bandwidth. The ray tracing simulation is followed by the development of the statistical model. It is observed that the reflection, diffraction and foliage losses increase with frequency.

Analysis of an OFDM based wireless broadband system which uses air-ground UAV links is presented in [13]. Experimental data is used to characterize the wireless broadband system. The UAV operates at a speed of 60 km/h and an altitude of 30 m. An adaptive 5×5 antenna array with vertical beam pattern is proposed for the air-ground link operating at 2.5 GHz. It is also observed that as the altitude increases, the data rate decreases.

In [14], a self configuring mesh network of micro UAVs is proposed and is simulated at the WLAN frequencies of 2.4 and 5.2 GHz. It considers microscopic, macroscopic and cluster movement of UAVs and assesses cognitive mobility models based on Received Signal Strength Identifier (RSSI). A log-normal channel is used to characterize slow fading for the inter-drone links operating at 30 to 800 m height in industrial and suburban areas and multipath fading is considered negligible at these operational heights.

The outage probability and bit rate are computed in [15] for a multi-carrier aerial relay using UAVs. Five different cases of varying fading parameters are considered and the channel model is computed analytically and the outage probability and BER are simulated. The simulations are performed at 2.4 GHz over a bandwidth of 80 MHz. At low altitudes and crowded areas, the Rayleigh fading model is considered and at higher altitudes, the Nakegami-m and Weibull fading as detailed in [16] are considered with large values of fading parameters.

The impact of ICI and noise on channel estimation is analyzed and the channel impulse response is obtained in [17]. It discusses the propagation aspects as in [9] having parking, taxi, arrival and en-route scenarios with a velocity of 440 m/s for the en-route scenario. A theoretical model is developed and the signal to interference ratio (SIR) is simulated with respect to the frequency of upto 6 GHz and the normalized ICI is analyzed. A two ray model as proposed in [9] has been used and it is found that the SIR in the en-route case decreases due to large Doppler shift as compared to the other scenarios. There is also a rapid decline of the SIR below 2 GHz and also decline of ICI.

In [18], the air-ground communications between a micro-UAV and the ground is considered. An altitude of 150 to 500 m is considered for the measurements. Balloons are also used upto 500 m height. Measurement data is compared with analytical and simulation results and coverage analysis is provided for cellular networks for both rural and urban environments. The measurements are performed at GSM and UMTS cellular frequencies of 900 MHz and 1.9 to 2.2 GHz. To model the propagation channel, the Okumara-Hata, COST-Hata and the COST Walfish-Ikegami model are considered. At higher altitudes, the multipath components in the near

vicinity of the ground are considered together with the LoS path and hence, the Friis formula with a path loss exponent of 2.5 is used to compute the pathloss. It is also observed that the common channel models used for terrestrial cellular communications are not useful for UAV air-ground links. In rural areas, it is observed that the received signal strength falls linearly with higher altitudes. The ray tracing results are useful for altitudes below 270 m height and the pathloss results are also comparable to the Okumara-Hata model.

From the above, the following inferences can be made:

- The altitude of the UAV determines the coverage area on the ground. Hence, the altitude is to be chosen such that only the required area is covered to avoid interference.
- The air-air relay channel has large Doppler shifts when the UAVs are operational and hence, the Doppler shift should be characterized and taken into account while designing the system. The coherence time is short and hence, the ICI is high.
- In characterizing the propagation channel models, a two ray model is proposed and Ricean distribution is used to characterize the multipath fading. The LoS component is characterized as a constant process and Rayleigh process is used to characterize the diffuse component.
- At high altitudes, the Weibull and Nakegami-m distributions with large values of fading parameters are used to characterize the fading.

4 Ray tracing analysis

4.1 Introduction to ray tracing

Characterization of the propagation channel can be performed computationally using either full wave electromagnetic simulations which are computationally intensive or ray tracing simulations which approximate ray theory for channel characterization at wireless communication frequencies. These simulations help in providing a basis for measurements as well as provide for statistical parameters regarding the channel.

In case of optics, the wavelength of the signal is very small and hence can be modelled as rays. Whenever the light ray intersects an object, due to the very small wavelength, the surface of the object appears rough to the incident wave and thus the light is scattered. When we consider microwave signals or signals with longer wavelengths compared to that of optical wavelengths, it is difficult to perform full-wave electromagnetic simulations to numerically solve for Maxwell equations considering the environment as the computational domain is very large. Hence, an approximation to optics is considered and ray-tracing methods are used to model the propagation scenarios.

In ray-tracing, the various paths which the signal takes from the transmitter to the receiver are considered. These paths primarily comprise of the direct path between the transmitter and the receiver, the specular reflected components from the obstacles and the diffracted components from sharp edges. The received electric field due to each of the components is computed with both the amplitude and phase and then combined to compute the received field at the receiver. To make the simulation results accurate, the effect of scattering and depolarization of the signal is to be taken into account.

The ray-tracing methods can be broadly classified into two major techniques namely the imaging method or the ray-launching method. In the imaging method, the various paths between the transmitter and the receiver are identified. The direction of the reflected wave from any surface is then computed based on the method of images. The overall received power is hence computed at the respective frequency thus determining the propagation characteristics. In the ray-launching method, rays are launched from the transmitter in all directions with a fixed angular separation and the path of the rays between the transmitter and the receiver is computed. The receiver is considered as a sphere whose radius depends on the Tx-Rx distance and the angular separation between two consecutive rays and all the rays passing through the sphere are considered to be received and hence, the total power at the receiver is calculated. This method is also computationally intensive and requires large amount of memory as the path of each ray needs to be identified. Characterizing diffracted rays results in a large number of new rays arising from the corresponding edge of the surface whose paths need to be traced resulting in increased complexity of the simulator.

4.2 Simulations

To model the propagation channel, ray tracing simulations were performed for different scenarios namely the Sendai City terrain, Japan and propagation over the sea at 2.4 GHz. The terrain used for modelling the Sendai City and sea are as shown in Figs. 9 and 10. In Sendai City terrain, there are hills at one end of the city with a height of about 150 m above the sea level. There are sparse amount of buildings closer to the hills and the other end of the city has an urban environment with buildings. The terrain is modelled such that the ground is electrically modelled as earth and the entire structure of the buildings is modelled as concrete. In a real environment, there will be vehicles, people on the terrain along with vegetation and trees which may result in variations between the simulations and the actual environment. Also, the buildings are modelled as rectangular blocks of a specified height hence is an approximation of the actual structure. This may result in deviations as the surface of buildings are not smooth in reality but have architectural designs. The material may also vary due to windows, wood, etc. which will not only change the electrical parameters but also scatter the incoming wave as the surface is no more smooth. This also results in depolarization of the incident wave. The surface of the sea is not smooth but modelled with waves.

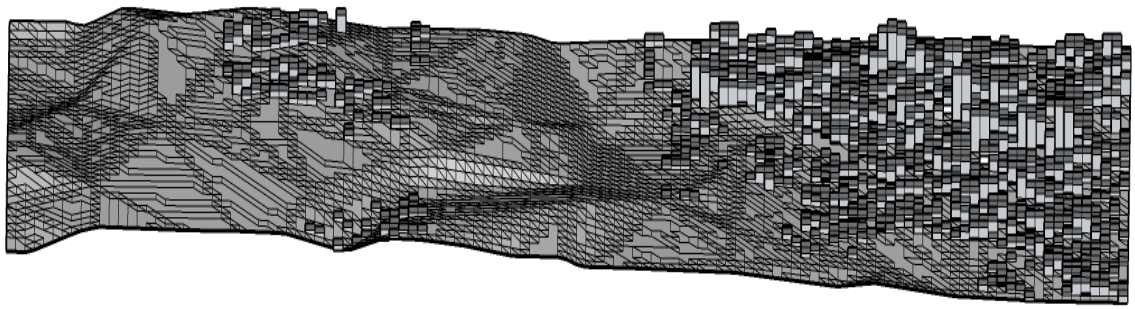

Fig. 9: Sendai terrain characteristics.

The simulations were performed at NICT, Japan and the data were processed for the thesis. For the purpose of simulations, the transmitter and receiver are considered as stationary and the channel was modelled at various locations along the movement of the UAV. The distance between the transmitter and receiver is about 3 km. The simulations are performed for 3 circular paths of the receiver UAVs as shown in Figs. 11 to 13 for both terrains. The UAVs are considered to be circling over the terrain with a radius of 100 m. The three circular receiver paths are located adjacent to each other. Assuming a stationary UAV, the transmitter locations are considered as fixed locations. There are 200 locations considered along each circular receiver path and 5 closely spaced transmitter locations with a separation distance of 1.25 m located approximately 3 km from the receiver are selected for the simulations. The ray-tracing simulations are then performed and the propagation characteristics are

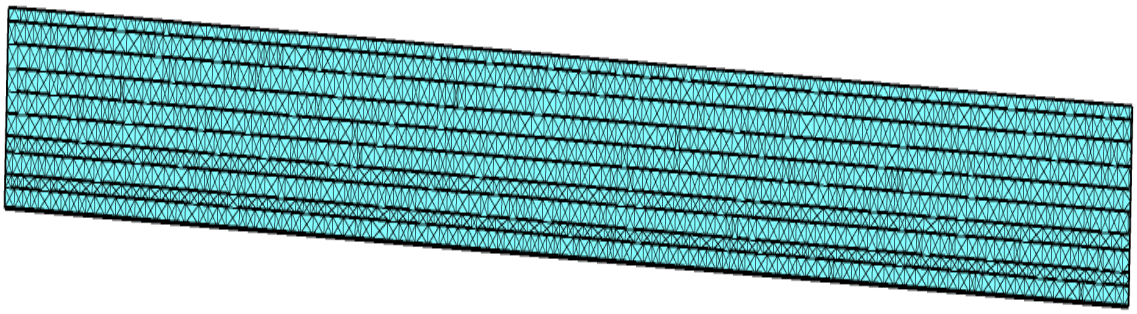

Fig. 10: Sea terrain characteristics.

obtained for all the Tx-Rx combinations between each of the 5 transmitter locations and all the receiver locations.

The operation of an aircraft or aerial vehicle is defined using the terrain level as a reference. Hence, the height of the UAV operation is based on the terrain. Thus if the two UAVs are operating such that one is operating above the plains and the other over a hilly terrain, then the actual altitudes of the UAVs will vary.

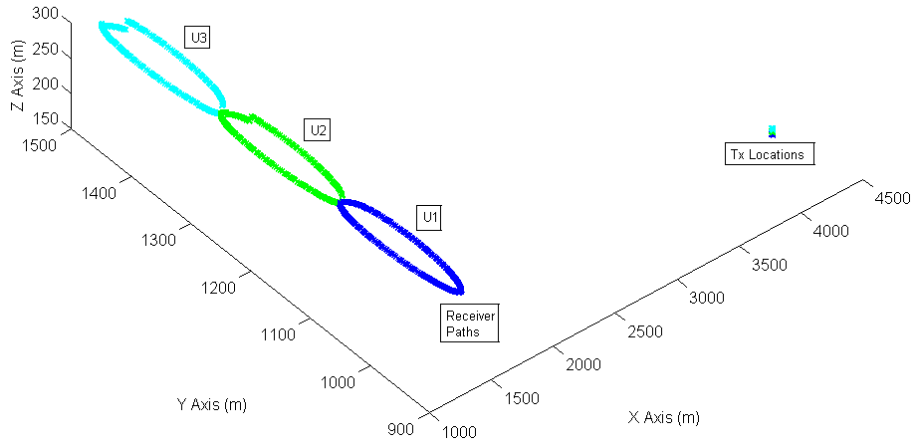

Fig. 11: UAV paths for Sendai City at 150 m height.

The simulations are performed using a commercial 3D ray tracing software, RapLab, developed by Kozo Keikaku Engineering (KKE) Inc., Japan. The ray tracing is performed using the imaging method over the terrain which is imported from the generated building information. The various paths between the transmitter and the receiver are considered and the corresponding path loss is computed for each path. The simulator takes into account the specular reflected components from the ground and the diffracted components based on uniform geometric theory of diffraction [3]. The simulator does not take into account the effect of scattering or the

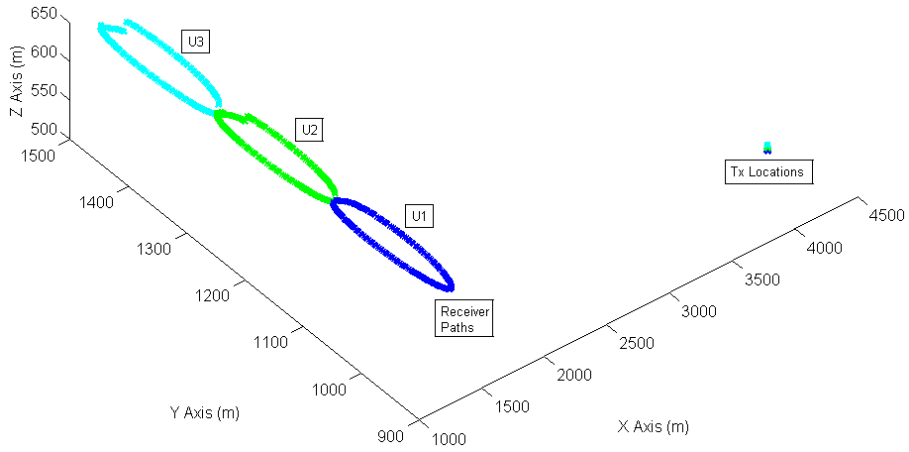

Fig. 12: UAV paths for Sendai City at 500 m height.

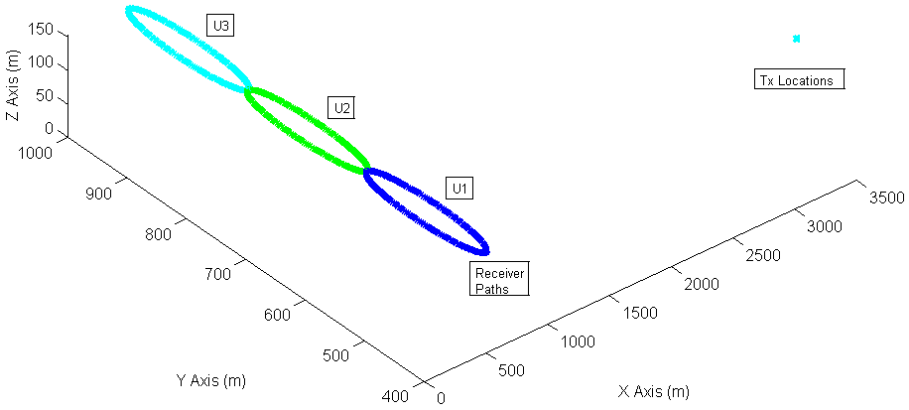

Fig. 13: UAV paths for over the sea scenario.

depolarization of the signal. The transmitter and receiver antennas are considered to be omnidirectional for the analysis and hence does not take into account antenna properties like directivity and polarization of the antennas. The reflection coefficients for the specular components are computed using the dielectric constant of the incident surface and the computed angle of incidence as given in Section 2.3. The formulas used for the computation of the reflection coefficient depend upon the polarization of the incident signal. The ray-tracing simulations are performed for Horizontal Tx-Horizontal Rx (H-H) and Vertical Tx-Vertical Rx (V-V) polarizations of the propagating wave.

5 Propagation channel modelling

5.1 Path loss model and small scale fading

The path loss model for the UAV-UAV communication link is created at 2.4 GHz from the simulated data using the least squared error (LSE) fit over the sea and Sendai city terrain at two heights of 150 m and 500 m above the terrain level for both H-H (Pol - 00) and V-V (Pol - 90) polarizations.

The simulations are performed for the scenario that the transmitter has fixed locations and the receiver is circling with a radius of 100 m at a distance of about 3 km from the transmitter. The path loss is computed for the corresponding Tx-Rx distances for H-H and V-V polarizations at 150 m and 500 m UAV heights. The pathloss model is created by averaging the pathloss over 10 m distances to remove the effect of small scale fading. It is then computed using the expression given in Section 2.8

$$PL(dB) = a(dB) + n10\log d, \tag{33}$$

where d is the Tx-Rx distance in metres, PL is the path loss for distance d, n refers to the path loss exponent which depends upon the environment clutter and a refers to the intercept which the LSE fit makes with the Y axis. The Y-intercept from the least squared error fit is considered instead of the close-in distance as the distances considered are only around 3 km.

Table 2: Path loss model parameters at 2.4 GHz for Sendai City terrain

Terrain	Height	Polarization	a	n	r^2	s^2
Sendai City	150 m	V-V	96.5831	3.2016	0.0241	4.1615
		H-H	69.1331	8.7395	0.5887	0.5341
	500 m	V-V	77.1882	7.0105	0.3918	0.7635
		H-H	98.1620	2.4121	0.8518	0.0101
Sea	150 m	V-V	77.4870	7.0952	0.0272	18.0074
		H-H	90.6647	4.1578	0.0287	5.8602
	500 m	V-V	63.7515	10.4555	0.1268	7.4171
		H-H	93.1437	3.6464	0.0583	2.1501

Table 2 provides the parameters for characterizing the path loss for all the scenarios with r^2 referring to the correlation coefficient to estimate the quality of the LSE fit and s^2 refers to the variance in error between the individual value and the LSE fit [19]. Figures 14 to 17 show the path loss for various paths for the different propagation scenarios. The LoS component is always available at the receiver without any shadowing. From Table 2, it is observed that although certain scenarios exhibit a higher pathloss exponent, their corresponding Y-intercept is lower. This is due to the fact that the Tx-Rx distances considered to model the pathloss model lie

between 2900 to 3150 km. In case of propagation over the sea at 150 m UAV height, the path loss is periodic in nature as shown in Fig. 16 and is indicative of the two-ray model.

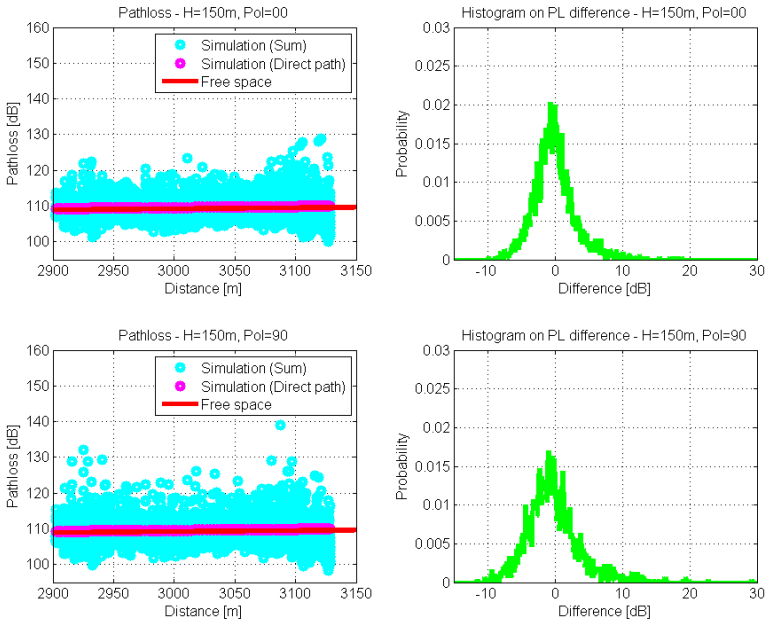

Fig. 14: Path loss characteristics for Sendai City terrain at 150 m height for H-H (Pol - 00) and V-V (Pol-90) polarizations.

The small scale fading for the propagation channel for different operating scenarios is characterized by Rician fading since there is a strong LoS path between the transmitter and receiver with reflected and diffracted components. The Rician K-factor is computed from the simulated data for various scenarios using Moment based estimation [20] to describe the strength of the direct component over the diffuse components. Fig. 18 shows the probability of the Rician K-factors for various scenarios over both the Sendai City and sea terrain. The receiver locations for computing the fading distribution characteristics are selected such that the received power lies within ± 3 dB of the mean signal strength for the selected path. This is done to select the paths which undergo the same propagation phenomenon for characterizing the small scale fading.

It is observed that the typical values for the Rician K-factor for propagation over the Sendai city terrain is maximum for the H-H polarization at 500 m (17 dB) while the K-factor for the other propagation scenarios is lower (between 10-14 dB) as shown in Fig. 18. The multipath components comprise primarily of diffracted paths or have multiple interactions having both reflection and diffraction while few paths undergo only reflection. The number of propagation paths decreases as the height increases. The strength of the multipath components is also lower for the 500 m height with

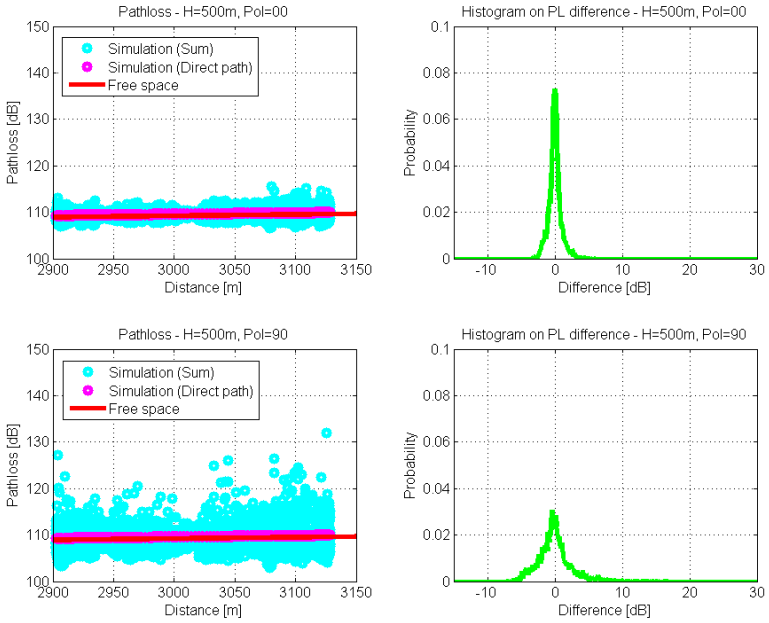

Fig. 15: Path loss characteristics for Sendai City terrain at 500 m height for H-H (Pol - 00) and V-V (Pol-90) polarizations.

H-H polarization of the signal. Hence, the K-factor is higher compared to the other propagation scenarios. The corresponding path loss is shown in Figs. 14 and 15. For propagation over the sea terrain, the typical value for the K-factor is between 10-12 dB. The fluctuation in the path loss over the sea can be seen in Figs. 16 and 17. The propagation phenomenon over the sea at both heights comprise of the LoS path, a reflected component and multiple diffracted components from the surface of the sea. The typical values for the K-factor lie between 10 to 15 dB for all the propagation scenarios.

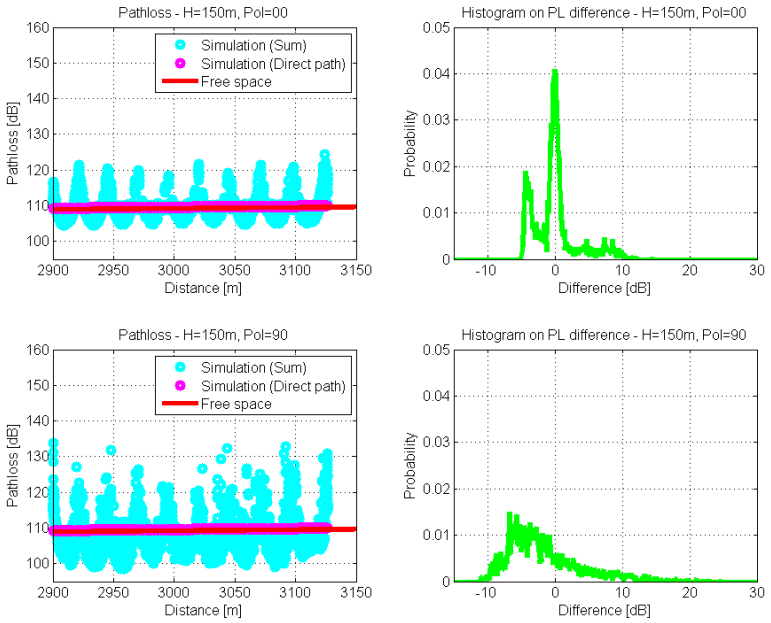

Fig. 16: Path loss characteristics for Sea terrain at 150 m height for H-H (Pol - 00) and V-V (Pol-90) polarizations.

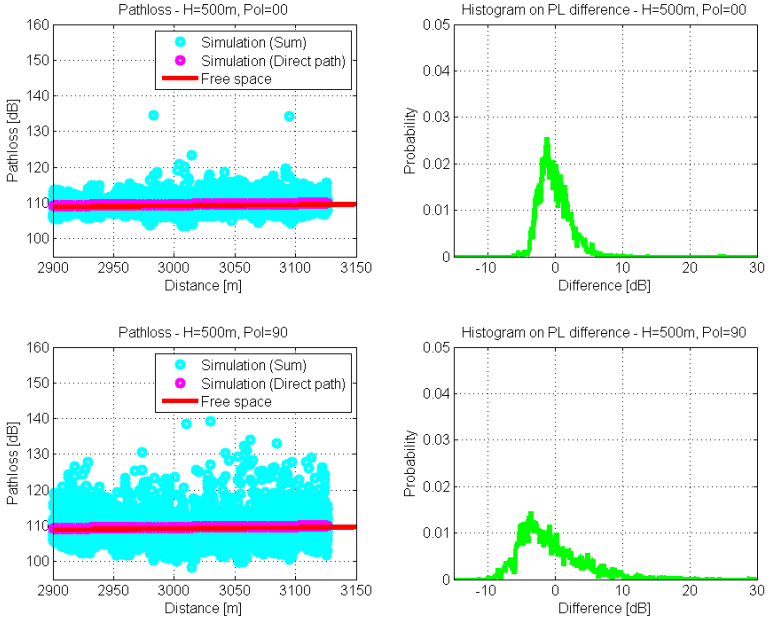

Fig. 17: Path loss characteristics for Sea terrain at 500 m height for H-H (Pol - 00) and V-V (Pol-90) polarizations.

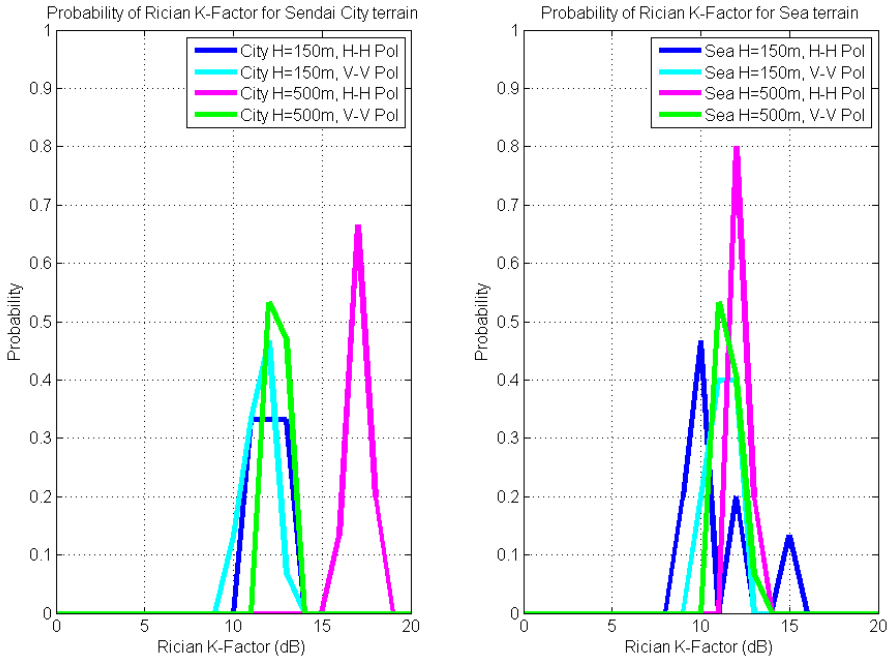

Fig. 18: Small scale fading - probability of Rician K-factors.

5.2 Delay dispersion

5.2.1 Excess delay

The excess delay of the multipath components arriving at a receiver with respect to the first arriving component is an important parameter for system design. For example, the design of OFDM systems require the specification of the guard interval between consecutive symbols so that intersymbol interference is avoided. Hence, characterization of the excess delay is an important requirement for system design. The signal strength of the delayed components is lower compared to that of the direct component due to the different phenomenon encountered by the corresponding component of the signal in its path.

The excess delay of the multipath components within 6, 12 and 18 dB below the direct component are considered for characterizing the propagation channel. The guard interval for 802.11 Wi-Fi systems is 800 ns with an optional guard interval of 400 ns for increased throughput [21] and the guard interval (cyclic prefix) for WiMAX systems depends on the symbol duration and can be varied as $\frac{1}{4}$, $\frac{1}{8}$, $\frac{1}{16}$ or $\frac{1}{32}$ of the symbol duration [22]. Hence, the system design should be such that the guard interval is sufficient to cover all the delayed multipath components of a given symbol.

The ray tracing simulations for both propagation over both the Sendai city terrain and sea provides the following results. Figs. 19, 20 and 21 show the excess delay for propagation at 150 m height above Sendai City for different UAV paths. It is observed that the excess delay for the H-H polarized components upto 18 dB below the direct path signal power varies between 37 to 55 ns for paths U1, U2 corresponding to an additional path length of 11.1 and 16.5 m respectively. The multipath components for the UAV paths U1 and U2 are similar with direct and ground reflected or diffracted rays. Due to the presence of hilly terrain and buildings, the height of the point of contact with the ground is higher than that of the sea level. For certain propagation paths, there are no multipath components upto 18 dB below the direct path and hence, only the direct path exists. When the receiver moves in path U2, for the V-V polarized signal, it can be observed that in addition to the delayed paths similar to those of horizontal polarization, there is an additional path with signal strength between 12 to 18 dB below the direct path at around 120 ns excess delay (additional path length 36 m) at some receiver locations. These types of path occurs due to an additional reflection occurring from the ground between the transmitter and receiver along with an initial diffraction as shown in Fig. 22, i.e., the ray interacts with two objects on the ground instead of a single object.

The propagation over receiver path U3 at 150 m height over the city provides for additional propagation paths between the transmitter and the receiver. Some multipath components are delayed by an excess delay of upto 460 ns for horizontal polarization of transmitting and receiving fields due to multiple interactions with objects on the ground between the transmitter and receiver as shown in Fig. 23. In case of V-V polarization of transmitting and receiving fields, for few paths, the

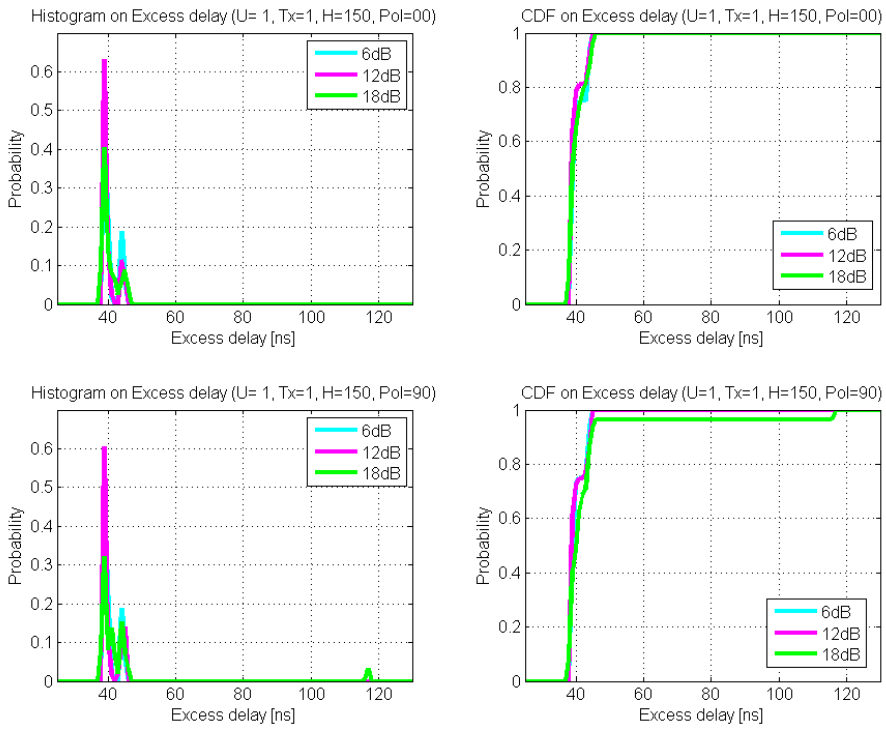

Fig. 19: Excess delay for UAV path U1 for H-H (Pol - 00) and V-V (Pol - 90) polarizations over Sendai City at H=150 m.

signal travels an additional distance of about 1 km beyond the transmitter as shown in Fig. 24 and undergoes both diffraction and reflection before arriving at the transmitter with a delay of 7.97 ms. These delayed paths have a signal strength between 12 to 18 dB below the direct component. These type of paths also occur for the H-H polarized propagation at 150 m height but the signal strength is lower than 18 dB below the maximum signal strength.

When the UAVs are operating at a height of 500 m above the ground over Sendai City, the excess delay varies between 490 to 570 ns as shown in Fig. 25 corresponding to an additional path length of 147 m and 170.9 m. The H-H polarized signal has only a multipath component 12 to 18 dB below the direct ray whereas the V-V polarized component has multipath components with signal strengths upto 18 dB below the direct component.

For the propagation over the sea at 500 m, there are rays which are reflected / diffracted (due to waves) from the surface of the sea along with the direct component which constitute the propagation paths between the transmitter and receiver. The excess delay of the multipath components varies between 523 to 568 ns and the signal strength upto 18 dB below the direct component for both H-H and V-V polarization. In case of V-V polarization, there are more paths with signal strength upto 6 dB below the direct component whereas they occur for very few paths in case of horizontal polarization. At 150 m height, the excess delayed component arrives

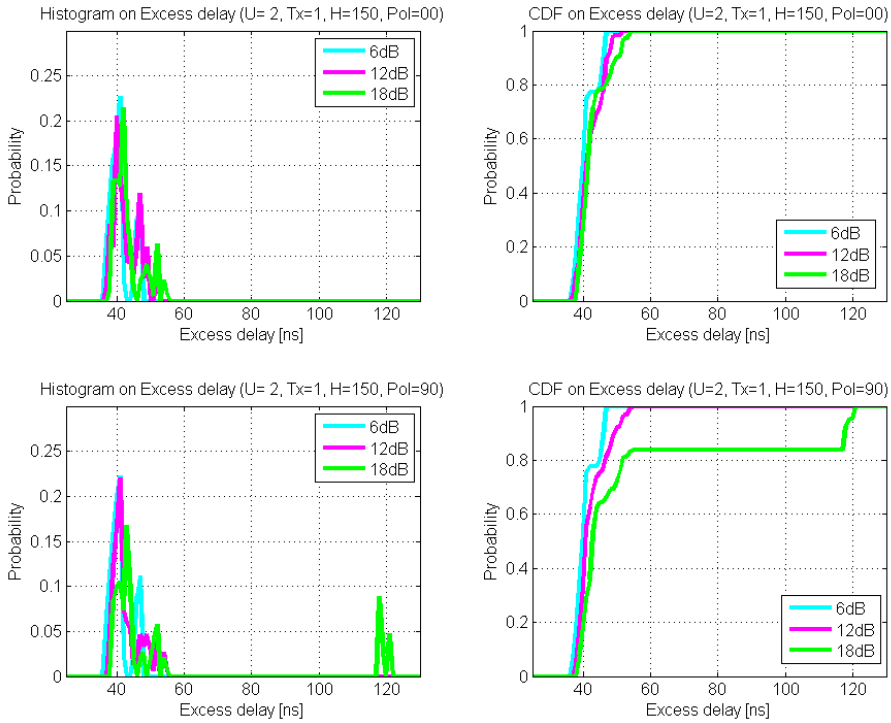

Fig. 20: Excess delay for UAV path U2 for H-H (Pol - 00) and V-V (Pol - 90) polarizations over Sendai City at H=150 m.

between 47 to 53 ns at the receiver due to ground reflections / diffractions from the sea level. The signal strength of the H-H polarized component is between 12 to 18 dB below the direct component whereas the signal level is higher for the V-V polarized multipath components with the excess delay varying upto 58 ns.

Hence, it is observed that when the propagation is over the Sendai City terrain, at larger heights (500 m), the strength of the multipath components is lower compared to that at 150 m. Although the excess delay is smaller for most scenarios at 150 m height, there are some paths with very large excess delays. In case of propagation over the sea, the multipath components for H-H polarization have lower signal strength as compared to the V-V polarization as shown in Figs. 26 and 27.

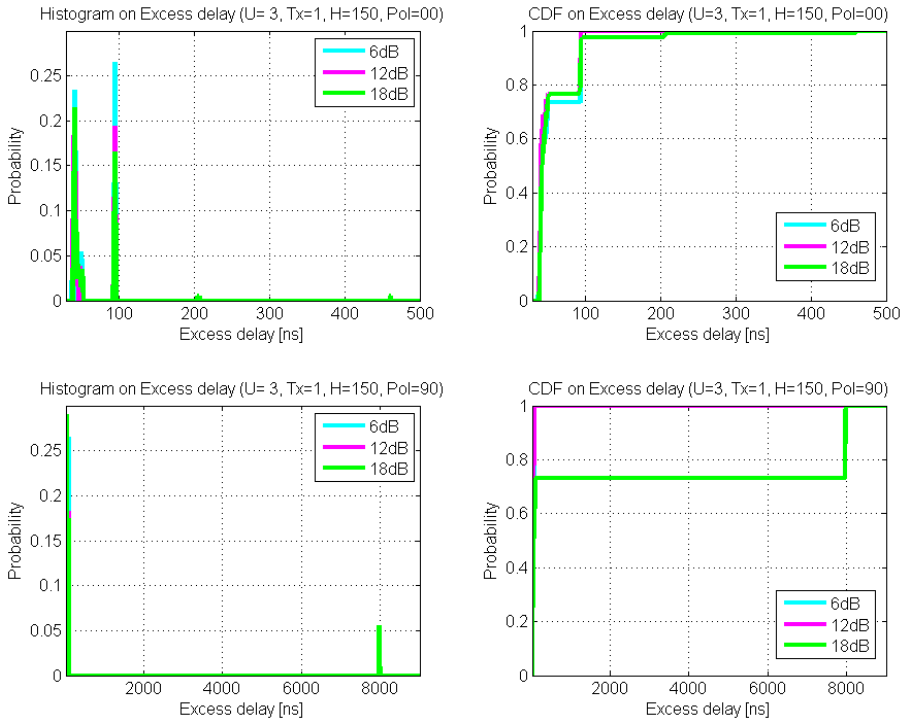

Fig. 21: Excess delay for UAV path U3 for H-H (Pol - 00) and V-V (Pol - 90) over Sendai City at H=150 m.

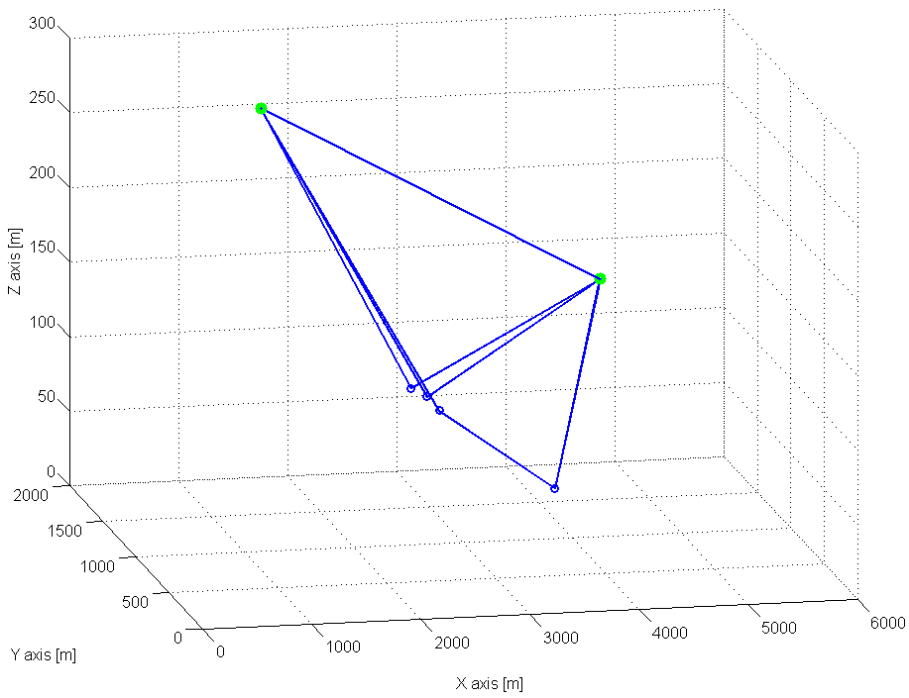

Fig. 22: Propagation paths for path U2 between Tx 1 and Rx 138 over Sendai City at H=150 m for V-V polarization.

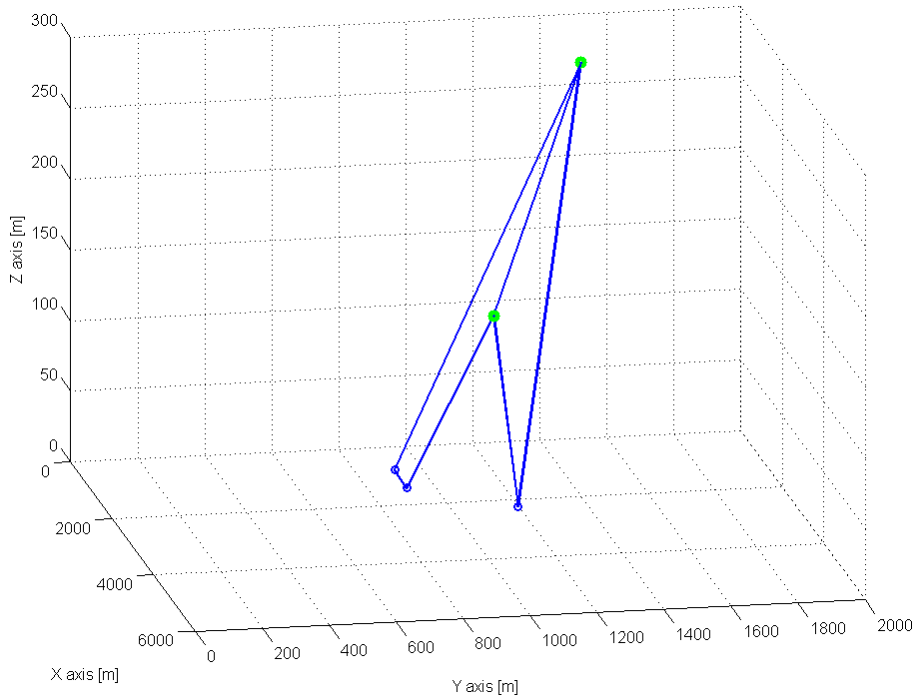

Fig. 23: Propagation paths for path U3 between Tx 1 and Rx 14 over Sendai City at H=150 m for H-H polarization.

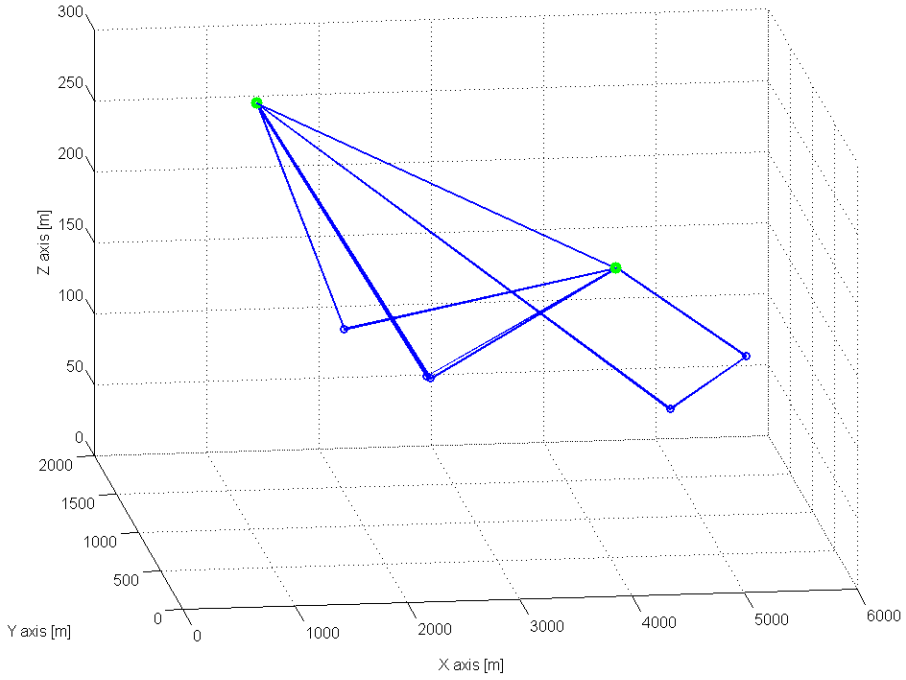

Fig. 24: Propagation paths for path U3 between Tx 1 and Rx 50 over Sendai City at H=150 m for V-V polarization.

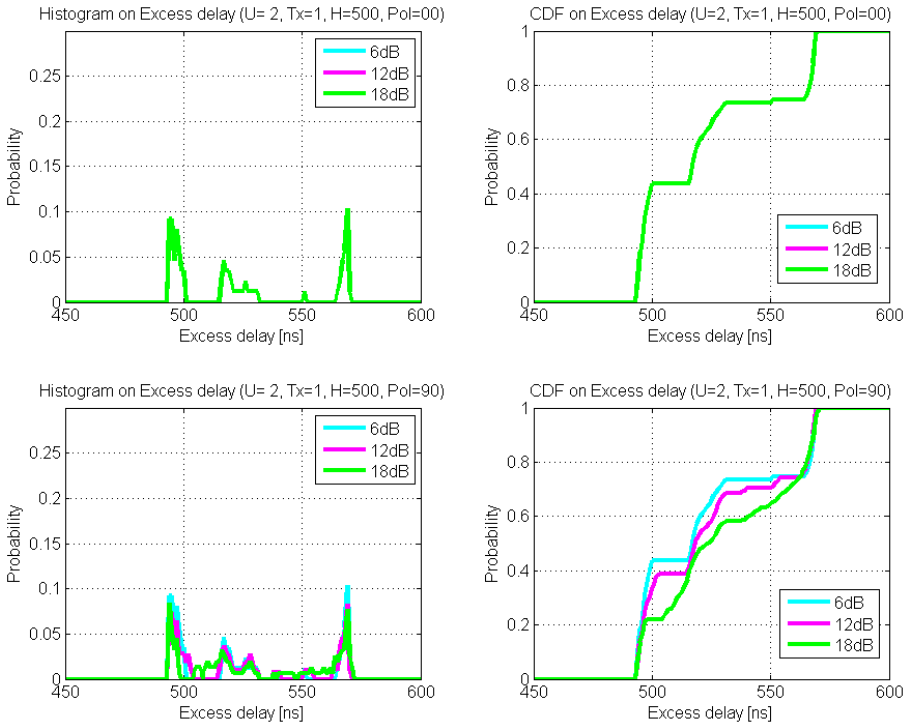

Fig. 25: Excess delay for UAV path U2 for H-H (Pol - 00) and V-V (Pol - 90) polarizations over Sendai City at H=500 m.

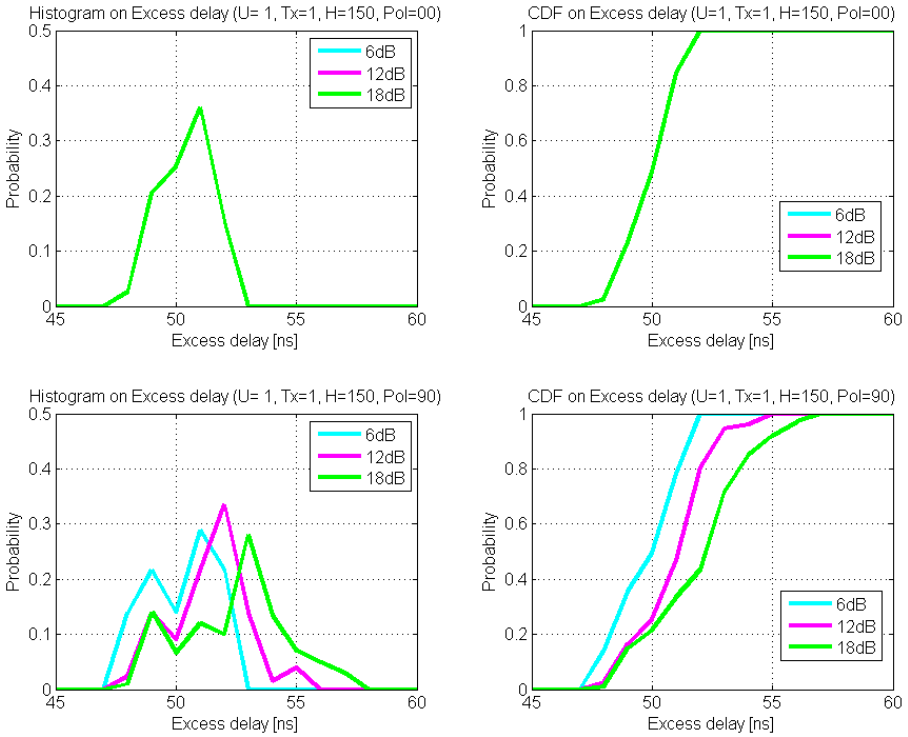

Fig. 26: Excess delay for UAV path U1 for H-H (Pol - 00) and V-V (Pol - 90) polarizations over the sea at H=150 m.

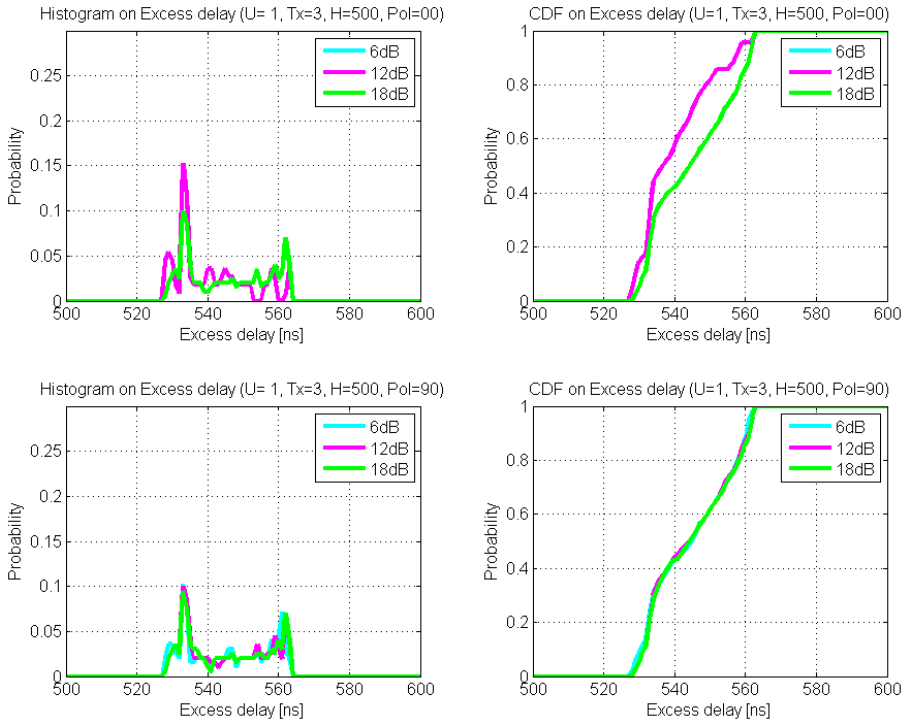

Fig. 27: Excess delay for UAV path U1 for H-H (Pol - 00) and V-V (Pol - 90) polarizations over the sea at H=500 m.

5.2.2 RMS delay spread

The RMS delay spread for various propagation scenarios is characterized to model the time dispersion. A power threshold of 30 dB below the signal strength of the direct component is used for the computation of the RMS delay spread. The coherence bandwidth, which determines the type of fading (flat or frequency selective) between two adjacent frequencies, is then determined for system design using the expressions in Section 2.11.3. The RMS Delay spread for the Sendai City terrain for the UAV paths U1 and U2 are similar with a maximum delay spread of 25 ns for H-H polarization and about 30 ns for V-V polarization as shown in Fig. 28. Due to the additional delayed paths for receiver path U3 as shown in Figs. 23 and 24, the delay spread is greater for UAV path U3 with a maximum delay spread of 1 ms for H-H and 1.7 ms for V-V polarizations. For propagation at 500 m height over the city, the delay spread varies upto 145 and 260 ns for H-H and V-V polarizations respectively for all the three receiver paths.

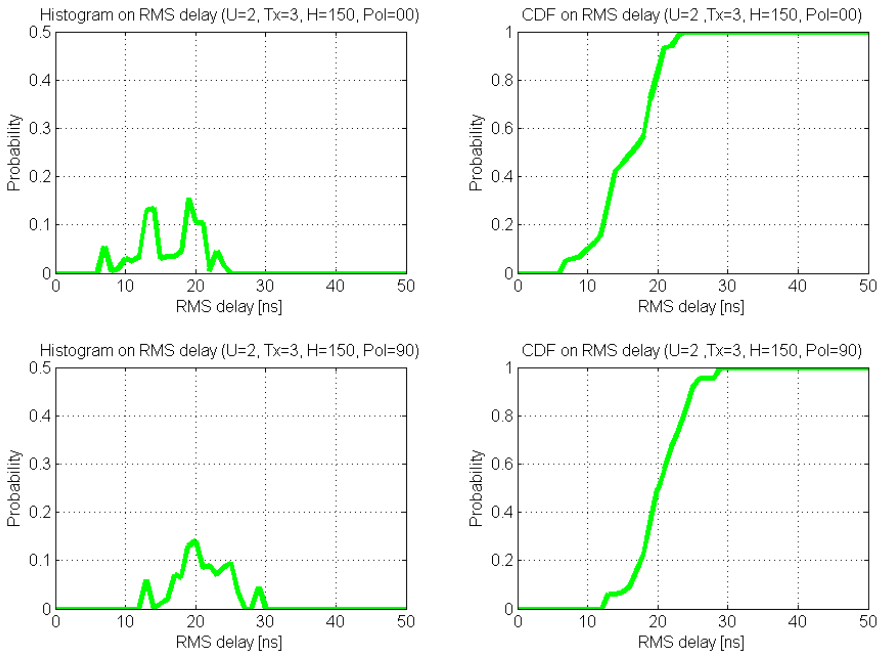

Fig. 28: RMS delay for UAV path U2 for H-H (Pol - 00) and V-V (Pol - 90) polarizations over Sendai City at H=150 m.

The RMS delay spread for propagation over the sea is similar for all three receiver paths. From Fig. 31, it is observed that the maximum delay spread is 262 and 278 ns respectively for both H-H and V-V polarizations respectively at 500 m height. The large RMS delay spread is due to the multipath signals with high signal strengths for both polarizations. In case of propagation at 150 m height, the peak RMS delay spread is at 23 and 25 ns for H-H and V-V polarizations respectively as shown in Fig. 32.

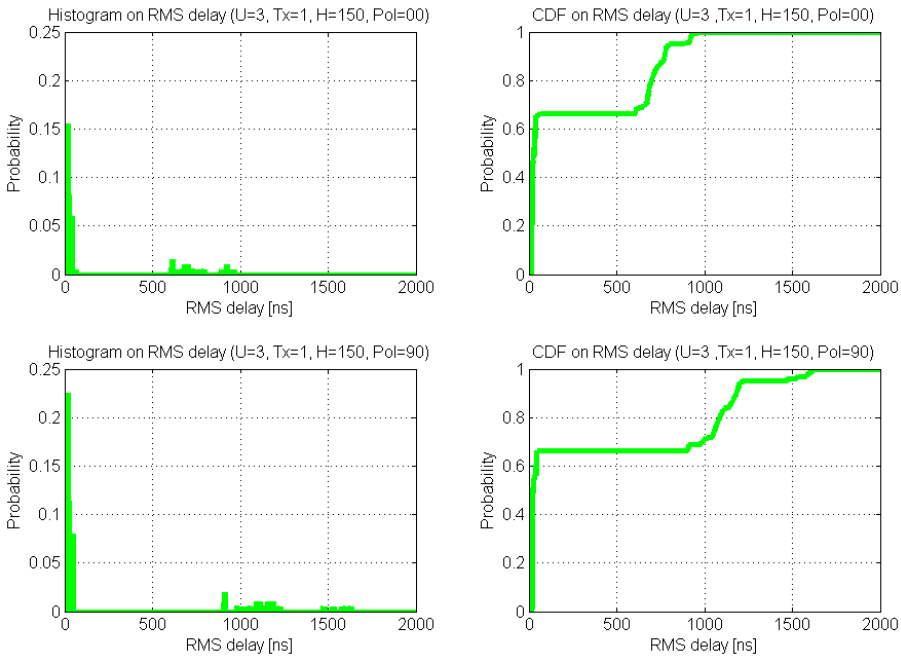

Fig. 29: RMS delay for UAV path U3 for H-H (Pol - 00) and V-V (Pol - 90) polarizations over Sendai City at H=150 m.

Table 3: RMS delay spread vs coherence bandwidth for correlation of 0.9

RMS delay	Coherence bandwidth
25 ns	800 kHz
30 ns	666.67 kHz
150 ns	222.22 kHz
270 ns	123.46 kHz
1000 ns	20 kHz
1700 ns	11.76 kHz

Table 3 shows the coherence bandwidth for a correlation of 0.9 for RMS delay spreads observed in the propagation between UAVs. It can be observed that the coherence bandwidth is typically very high for propagation at 150 m height as the RMS delay spread is very small. The coherence bandwidth is very small for a few propagation paths in UAV path U3 due to multipath components with significant signal strengths. The sub-carrier spacing of OFDM systems is compared to the coherence bandwidth to predict the type of frequency fading in the channel. In case of 802.11 Wifi systems, the sub-carrier frequency spacing is 312.5 kHz for OFDM [21]. For 802.16 WiMAX with a channel bandwidth of 10 MHz and 1024 point FFT for OFDM [22], the sub-carrier spacing is 10.94 kHz. Hence, it can be seen that even in the worst case scenario (RMS delay spread of 1700 ns), the sub-carrier spacing of WiMAX systems is smaller than the coherence bandwidth. Hence, the

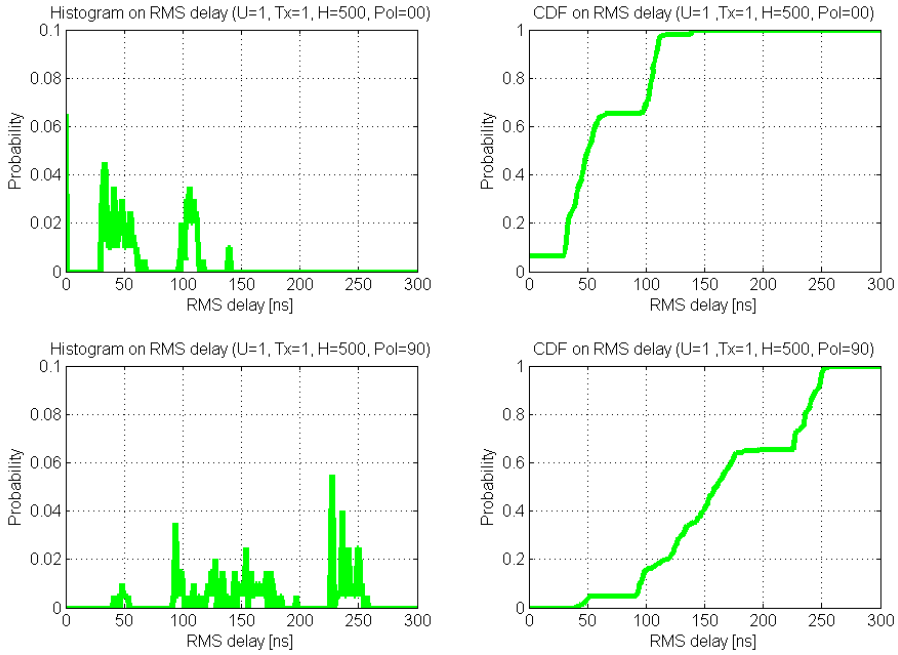

Fig. 30: RMS delay for UAV path U1 for H-H (Pol - 00) and V-V (Pol - 90) polarizations over Sendai City at H=500 m.

frequency selective fading channel can be divided into multiple sub-carriers undergoing frequency flat fading. In case of 802.11g/n systems, due to the large sub-carrier spacing of 312.5 kHz, only transmissions at 150 m UAV height excluding the worst case scenario (RMS delay spread of 1700 ns) have sub-carriers which undergo frequency flat fading while all other scenarios exhibit frequency selective fading for the sub-carriers.

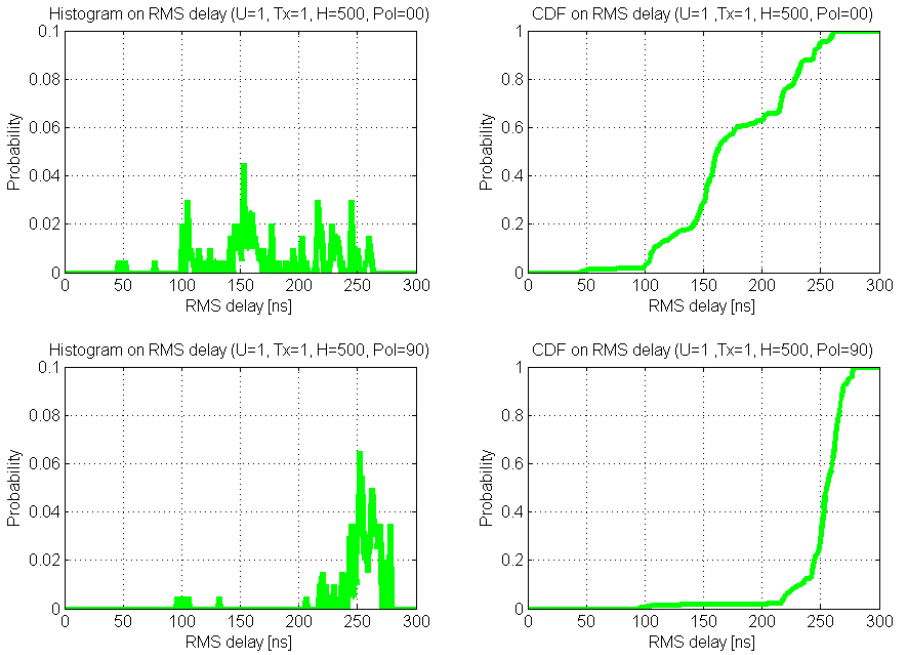

Fig. 31: RMS delay for UAV path U1 for H-H (Pol - 00) and V-V (Pol - 90) polarizations over the sea at H=500 m.

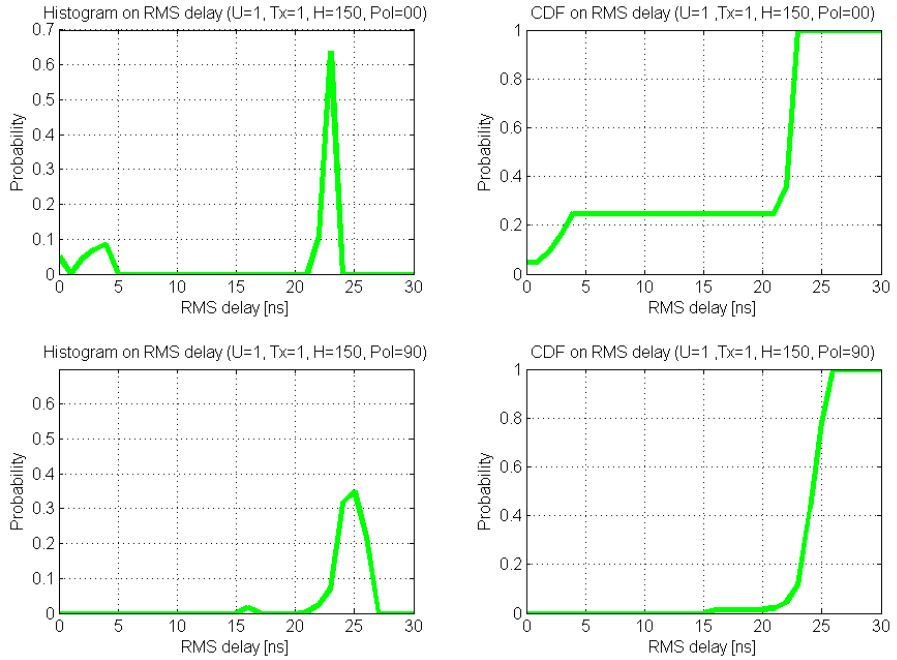

Fig. 32: RMS delay for UAV path U1 for H-H (Pol - 00) and V-V (Pol - 90) polarizations over the Sea at H=150 m.

5.3 Doppler dispersion

The Doppler spread of the frequency during propagation of the two UAVs depends upon the speed at which the UAV operates. Consider the UAVs to be communicating at 2.4 GHz and operating with a speed of 120 to 180 kmph (33.3 to 50 m/s). Since the UAVs, move in a circular path, during one half of the path, the receiver will be moving away from the transmitter and during the other half, it will be moving towards the transmitter. Hence, the Doppler shift occurs on both sides of the center frequency. Considering the maximum speed of operation of the UAVs at 2.4 GHz, the maximum Doppler shift is computed as 266.4 and 400 Hz for 120 and 180 km/h speeds respectively. When the UAV is operating at its maximum speed, the frequency spreads over a bandwidth of 800 Hz.

The Doppler spread varies for different multipath components arriving at the receiver. For simplicity, the angle of arrival of the received components is considered in the elevation plane for all the propagation scenarios as shown in Fig. 33. As the angle of arrival of the LoS component is close to the azimuth plane, it undergoes maximum Doppler shift depending upon the direction of motion of the UAV. It is observed that the angle of arrival of the multipath components is of very narrow beamwidth except for propagation over the Sendai City at 500 m UAV height. If the receiver is considered to be moving at constant elevation in the azimuthal plane, the angle of arrival and hence, the angle between the direction of motion of the UAV and the multipath component lies within the specified beamwidth. The corresponding Doppler shifts of the multipath components for different scenarios is given in Table 4. The direction of frequency shift depends upon the direction of motion of the UAV.

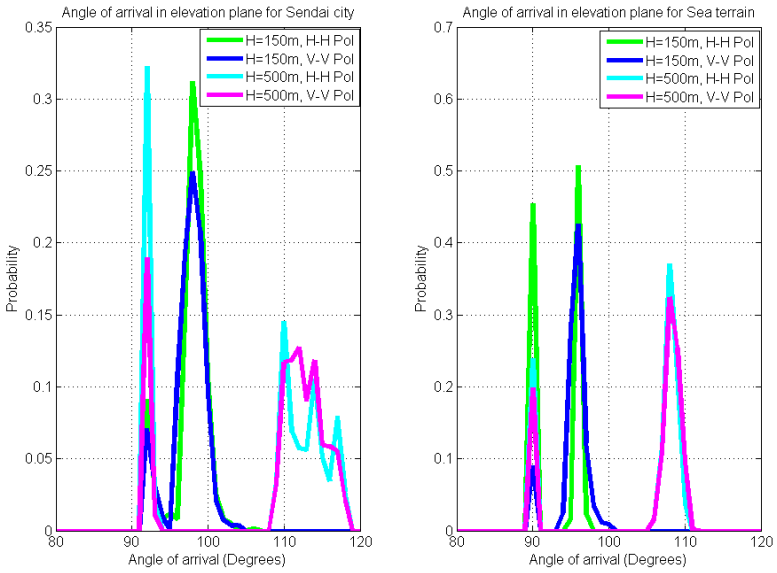

Fig. 33: Angle of arrival in elevation plane.

Table 4: Doppler shift of the multipath components for 50 m/s UAV speed

Terrain	Height	Polarization	Angle of arrival	Doppler shift (Hz)
Sendai City	150 m	V-V	96° - 104°	388.12 - 397.81
		H-H	96° - 106°	384.5 - 397.81
	500 m	V-V	109° - 118°	353.18 - 378.21
		H-H	109° - 118°	353.18 - 378.21
Sea	150 m	V-V	94° - 100°	393.92 - 399.03
		H-H	95° - 97°	398.48 - 397.92
	500 m	V-V	106° - 110°	375.88 - 384.5
		H-H	106° - 110°	375.88 - 384.5

The sub-carriers in OFDM systems are sensitive to Doppler shift. A shift in the sub-carrier frequency affects the carrier spacing and hence the symbol duration which is inversely proportional to it. This results in ICI in adjacent sub-carriers [23],[24]. The product of the Doppler shift (f_d) and symbol duration (T_s)is used to characterize the impact of frequency dispersiveness of the channel. The symbol duration of 802.11g systems is 4 μs and 3.6 μs for systems with shorter guard interval. This results in an $f_d T_s$ of 0.0016 and 0.0014 respectively. In case of 802.16e with a 1024 point FFT and 10 MHz bandwidth, the symbol duration is 91.4 μs which results in an $f_d T_s$ of 0.036. Due to the larger values of $f_d T_s$ for 802.16 systems (> 0.01), synchronization errors may occur resulting in shifting of the local oscillator frequency at the receiver thereby resulting in ICI.

6 Conclusion

The aim of the thesis was to characterize the propagation channel between UAV relays to establish reliable communication systems for deployment during emergency scenarios. The possibility of deploying such unmanned airborne systems is gaining traction especially by regulatory authorities and governmental agencies to provide communication to the users in the affected region.

In the thesis, first, the background and need for establishing UAV communications in emergency scenarios was established describing the challenges and requirements. The necessity of modelling the propagation channel between the UAVs for aerial links was also established with the requirements for modelling the channel. Then, the basic propagation mechanisms and the theory behind modelling the propagation channel have been discussed in Chapter 2 followed by discussion on UAV communications with emphasis on UAV-UAV relay links in Chapter 3. Previous work done to describe the propagation channel model were discussed in detail to obtain background information for the channel analysis.

Then, ray tracing analysis was performed at 2.4 GHz using the imaging method using a RapLAB, a commercial ray-tracing simulator at NICT, Japan for propagation over the Sendai City terrain in Japan and over the sea. The ray tracing simulations were performed at 150 m and 500 m height above the terrain level as described in Chapter 4 to understand the effect of the height on the propagation channel and the effect of propagation of both horizontal - horizontal and vertical - vertical polarizations were analyzed.

The propagation channel was modelled for the simulated scenarios and the results were described in Chapter 5. The major parameters to characterize the channel, i.e. the path loss model, small scale fading, RMS delay spread, excess delay and Doppler spread were analyzed for the the different propagation scenarios. The path loss for the different scenarios were analyzed and the path loss for each Tx-Rx combination was computed and found to be close to the free space path loss as the LoS component is always available at the receiver. The small scale fading which occurs due to the presence of multiple paths between the transmitter and the receiver is then characterized using the Rician distribution. In case of propagation over Sendai City, propagation at 500 m height with H-H polarization provides with typical K-factor of 17 dB while the other scenarios have lower K-factors indicating the stronger effect of multipath components. In case of propagation over the sea, the K-factor typically varies between 10-12 dB. The delay dispersion was then analyzed and both the excess delay and RMS delay spread for the different scenarios were discussed. The excess delay of the multipath components shows that at lower UAV heights, the signal strength of the delayed components is higher due to large number of diffracted paths. The typical excess delay is lower at 150 m height due to the small additional distance travelled by the multipath components but certain propagation paths in Sendai City scenario have very large excess delay due to undergoing multiple inter-

actions with objects on the ground. At larger heights of 500 m, the propagation phenomenon is similar for all paths and hence, all the excess delayed paths arrive within the 570 ns for a propagation distance of about 3 km. The signal strengths of the delayed multipath components is lower for the H-H polarized components than that of the V-V polarized components. Then the effect of Doppler shift based on the UAV operating speeds was discussed.

Table 5: Summary of crucial parameters for channel modelling

Terrain	Sendai City				Sea			
UAV Height	150 m		500 m		150 m		500 m	
Polarization	H-H	V-V	H-H	V-V	H-H	V-V	H-H	V-V
Pathloss Y-intercept	69.13	96.58	98.16	77.19	90.66	77.49	93.14	63.75
Pathloss exponent	8.74	3.2	2.41	7.01	4.16	7.1	3.64	10.46
Ricean K-factor	11-13 dB	10-12 dB	16-18 dB	12-13 dB	9-15 dB	9-12 dB	12-13 dB	11-13 dB
Excess delay 12 dB	95 ns	95 ns	-	570ns	-	55 ns	565 ns	565 ns
Excess delay 18 dB	461 ns	7970 ns	570 ns	570 ns	52 ns	57 ns	565 ns	565 ns
RMS delay spread	1000 ns	1700 ns	145 ns	260 ns	24 ns	26 ns	260 ns	280 ns

A summary of the crucial parameters required for modelling the Sendai City and the sea terrain are listed in Table 5. The transmitted power for communication systems should be such that sufficient margin is available to overcome pathloss and fading. The guard interval of 802.11g systems (800 ns) is sufficient for most propagation scenarios except when propagation paths have long excess delays (Sendai City UAV path U3) while the optional 400 ns guard interval is not sufficient for transmission at larger UAV heights (500 m). The guard interval (cyclic prefix) of 802.16 WiMAX can be selected to overcome the excess delayed paths for all the scenarios. The sub-carrier spacing for WiMAX systems can be designed for frequency flat fading for each sub-carrier and with frequency selective fading over the entire channel. The same is applicable for 802.11 OFDM systems only for propagation at lower UAV heights (150 m) without considering the worst case scenario of certain paths in Sendai city terrain for UAV path U3. Due to the large symbol duration of 802.16 systems, there may be synchronization errors resulting in ICI whereas this is not a major concern for 802.11 systems due to their comparatively smaller symbol durations.

6.1 Future work

Although simulations have been performed to obtain an understanding of the propagation phenomenon and channel characteristics for the UAV-UAV relay links, measurements are required to validate the simulated data. Measurements are to be done

in Hawaii, USA with corresponding ray-tracing simulations to validate the simulations as well as to develop a final propagation model for system design. The designed propagation model is then used to design communication systems for the relay links to provide communication in disaster struck areas.

References

[1] "The role of deployable aerial communications architecture in emergency communications and recommended next steps," in *2011 White Paper: Public Safety and Homeland Security Bureau*, Washington DC, Sep. 2011.

[2] Workshop on deployable aerial communications architecture, *http://www.fcc.gov/events/workshopwebinar-deployable-aerial-communications-architecture, 20/05/2012,* Washington DC, Oct 2011.

[3] S. R. Saunders and A. Aragon-Zavala, *Antennas and Propagation for Wireless Communication Systems,* 2nd Edition, Chichester, England, John Wiley & Sons Ltd., 2007.

[4] T. S. Rappaport, *Wireless Communications - Principles and Practice,* 2nd Edition, New Jersey, USA, Pearson Education Inc, 2002.

[5] H. L. Bertoni, *Radio Propagation for Modern Wireless Systems,* New Jersey, USA, Prentice-Hall PTR, 2000.

[6] J. D. Parsons, *The Mobile Radio Propagation Channel,* 2nd Edition, Chichester, England John Wiley & Sons, Inc., 2001.

[7] "Electrical characteristics of the surface of the earth," in *Recommendation ITU-R, P.527-3*, Geneva, Switzerland, 1992.

[8] "Unmanned aerial vehicle," in *The Free Dictionary, http://www.thefreedictionary.com/Unmanned+Aerial+Vehicle, 20-05-2012.*

[9] E. Haas, "Aeronautical channel modeling," *IEEE Transactions on Vehicular Technology*, vol. 51, no. 2, pp. 254–264, March 2002.

[10] S. M. Elnoubi, "A simplified stochastic model for the aeronautical mobile radio channel," in *Proc. 42nd IEEE Vehicular Technology Conference (VTC '92)*, vol. 2, Denver, USA, May 1992, pp. 960–963.

[11] W. Zhiqiang, H. Kumar and A. Davari, "Performance evaluation of OFDM transmission in UAV wireless communication," in *Proc. 37th Southeastern Symposium on System Theory (SSST '05)*, Tuskegee, AL, Mar. 2005, pp. 6–10.

[12] Q. Feng, J. McGeehan, E.K. Tameh and A.R. Nix, "Path loss models for air-to-ground radio channels in urban environments," in *Proc. 63rd IEEE Vehicular Technology Conference (VTC '06-Spring)*, vol. 6, Melbourne, Australia, May 2006, pp. 2901–2905.

[13] P. Park, S. Choi, D. Lee and B. Lee, "Performance of UAV communication system adapting WiBro with array antenna," in *Proc. 11th International Conference on Advanced Communication Technology (ICACT '09)*, vol. 2, Gangwon-Do, South Korea, Feb. 2009, pp. 1233–1237.

[14] K. Daniel, S. Rohde, N. Goddemeier and C. Wietfeld, "Fading countermeasures with cognitive topology management for aerial mesh networks," in *Proc. 2010 IEEE International Conference on Wireless Information Technology and Systems (ICWITS '10)*, Hawaii, USA, Aug. 2010, pp. 1–4.

[15] I.Y. Abualhaol and M.M. Matalgah, "Performance analysis of multi-carrier relay-based UAV network over fading channels," in *Proc. 2010 IEEE GLOBECOM Workshops (GC Wkshps '10)*, Miami, FL, USA, Dec. 2010, pp. 1811–1815.

[16] M.K. Simon and M.S. Alouini, *Digital Communication over Fading Channels,* 2nd Edition, New Jersey, USA, John Wiley & Sons, 2005.

[17] H. Jian, and Z. Yue-tong, "Impact of Doppler on high speed UAV OFDM system," in *Proc. 2009 International Conference on Communication Software and Networks (ICCSN '09)*, San Fransisco, USA, Feb. 2009, pp. 742–745.

[18] N. Goddemeier, K. Daniel, and C. Wietfeld, "Coverage evaluation of wireless networks for Unmanned Aerial Systems," in *Proc. 2010 IEEE Globecom Workshop on Wireless networking for Unmanned Aerial Vehicles (GC Wkshps '10)*, Miami, FL, USA, Dec. 2010, pp. 1760-1765.

[19] "Least Squares Fitting," in *Wolfram MathWorld, http://mathworld.wolfram.com/LeastSquaresFitting.html, 19-12-2012.*

[20] L. J. Greenstein, D. G. Michelson, and V. Erceg, "Moment-method estimation of the Ricean K-factor," in *IEEE Communication Letters*, vol. 3, no. 6, pp. 175–176, June 1999.

[21] "IEEE Standard for Information technology–Telecommunications and information exchange between systems Local and metropolitan area networks–Specific requirements Part 11: Wireless LAN Medium Access Control (MAC) and Physical Layer (PHY) Specifications," in *IEEE Std 802.11-2012 (Revision of IEEE Std 802.11-2007)*, pp. 1–2793, March 2012.

[22] "IEEE Standard for Air Interface for Broadband Wireless Access Systems," in *IEEE Std 802.16-2012 (Revision of IEEE Std 802.16-2009)*, pp. 1–2542, August 2012.

[23] A. F. Molisch, *Wireless Communications,* 2nd Edition, Chichester, England, John Wiley & Sons, Ltd., 2005.

[24] P. Robertson and S. Kaiser, "The effects of Doppler spreads in OFDM(A) mobile radio systems," in *Proc. 50th IEEE Vehicular Technology Conference (VTC 1999-Fall)*, vol. 1, Amsterdam, Netherlands, September 1999, pp. 329–333.